AD NUMBER

AD874649

NEW LIMITATION CHANGE

TO

Approved for public release, distribution unlimited

FROM

Distribution authorized to U.S. Gov't. agencies and their contractors; Critical Technology; JUN 1970. Other requests shall be referred to Air Force Inst. of Technology, Wright-Patterson AFB, OH 45433.
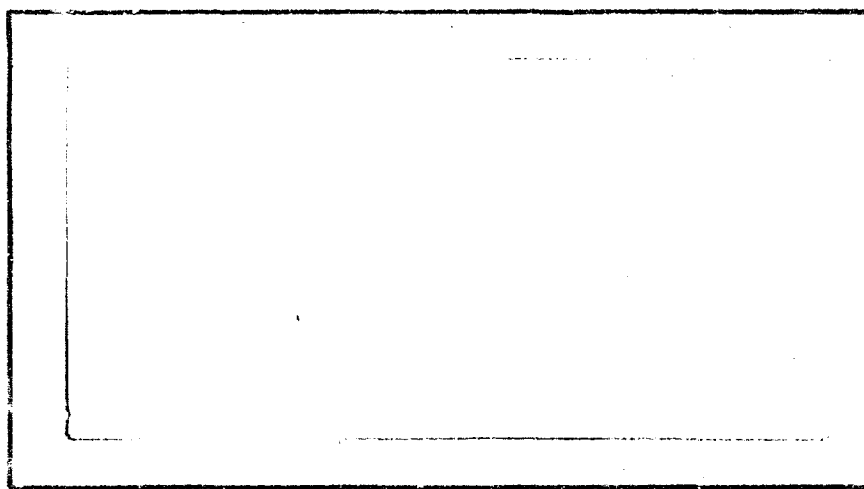
AUTHORITY

AFIT ltr, 22 Jul 1971

AIR FORCE INSTITUTE OF TECHNOLOGY

AIR UNIVERSITY
UNITED STATES AIR FORCE

SCHOOL OF ENGINEERING

WRIGHT-PATTERSON AIR FORCE BASE, OHIO

COHERENCE PROPERTIES OF A

PULSED RUBY LASER

THESIS

GSP/PH/70-12   Thurston C. Holley
                               Captain   USAF

COHERENCE PROPERTIES OF A

PULSED RUBY LASER

THESIS

Presented to the Faculty of the School of Engineering

of the Air Force Institute of Technology

Air University

In Partial Fulfillment of the

Requirements for the Degree of

Master of Science

by

Thurston C. Holley, B.S.E.E.

Captain   USAF

Graduate Space Physics

June 1970

Preface

At the time of this study, there was very little material published concerning procedures to be used to analyze the coherence properties of pulsed, multi-moding solid state lasers. Consequently, the experimental procedures adopted were based on methods used successfully to analyze conventional sources. As a result, refinements in these procedures became apparent as the study progressed. These refinements are presented in the discussions of each experiment.

My motivation for choosing this problem is more than the satisfaction of the degree requirement and a genuine fascination for high power lasers. I hope that the coordination required of the various Air Force laboratories and AFIT as students pursue thesis problems in coherent optics applications, will result in better preparation of students in this area by AFIT and an enlargement in the commitment to this area by Air Force laboratories. Considering the multitude of potential, Air Force applications of holography (non-destructive testing, simulators, holographic radar, etc.) and the holographic expertise here at Wright-Patterson, it is my opinion, that an elective course in holography would pay many dividends to the Air Force.

Now I would like to express my gratitude to the many individuals who assisted me during this study. First, I would like to thank my laboratory adviser, Tom Williamson, for the continuous aid he provided which ranged from explanation of extremely difficult concepts to suggestions concerning illustrations. Also I would like to thank Harold W. Rose and Richard L. Remski for the many discussions we had.

ii

These discussions proved to be invaluable for the careful analysis attempted in this study. Next, I would like to express my gratitude to Charles H. Stevens for helping me solve many logistic problems when the situation appeared hopeless. Also I would like to thank John Edson and C. Richard Lane for their assistance with the photographic work.

Next I would like to thank Dr. Leno S. Pedrotti, Colonel Paul A. Whelan, and Captain Kendall F. Casey, Jr., for the many helpful comments concerning the written report. And finally I would like to thank the people at the Avionics Laboratory for the use of their facilities and equipment and the excellent support they gave me.

                                        Thurston C. Holley

GSP/PH/70-12

Contents

List of Figures

List of Symbols

$U(x_1, y_1)$ Complex amplitude in the (x_1, y_1)-plane

$RECT(x) = \begin{cases} 1, & |x| \leq 1/2 \\ 0, & \text{Otherwise} \end{cases}$ Generalized function

$SINC(x) = \dfrac{SIN\ \pi\ x}{\pi\ x}$

Δ_o Physical thickness of a thin lens at its center

f Focal length of a thin lens

n Refractive index

$K = \dfrac{2\pi}{\lambda}$ Wave number

$J = \sqrt{-1}$

$\mathscr{F}\{\ \}$ Fourier transform

$B\{\ \}$ Zero order Hankel transform

$*$ Convolution

f_x, f_y Spatial frequencies

$C(\alpha), S(\alpha)$ Fresnel integrals

$CIRC\ r = \begin{cases} 1, & |r| \leq 1 \\ 0, & \text{Otherwise} \end{cases}$ Generalized function

γ_{12} Complex degree of spatial coherence

σ Secondary source – Chapter II

V Intensity visibility

$V' = (V)^{1/2}$ Amplitude visibility

$\tau = \dfrac{I_{out}}{I_{in}}$ (Local Ave)   Intensity transmittance

γ Slope of Hurter-Driffield Curve

E Exposure

D	Photographic density
$t = \dfrac{U_{out}}{U_{in}}$	Amplitude transmittance
r	Reflectance
$\delta = K(x_2 - x_1)$	Optical path difference
$\sigma = \dfrac{1}{\lambda}$	Chapter III
J_{21}	Total coherence function
Δt	Coherence time
ΔL	Coherence length

Abstract

The output power and pulse duration of the pulsed ruby laser
satisfies the requirements needed to holographically record moving
scenes. Thus the purpose of this study is to evaluate the coherence
properties of the laser as a possible holographic source.

The spatial coherence was determined by performing a form of
Young's experiment. The interference fringes were recorded on photo-
graphic emulsion and scanned by a densitometer. The relative inten-
sities of the recorded fringes were then determined with the aid of
the Hurter-Driffield curves for the different emulsions used. For an
aperture radius of 0.51 millimeters, the spatial coherence length was
found to be approximately 2.2 millimeters. Also the experimental
results were compared with a theoretical prediction.

The degree of temporal coherence was determined with the aid of
a Twyman-Green interferometer. The relative intensities of the
recorded fringes were determined in the same manner as before. A
temporal coherence length of 1.27 centimeters was observed. A single
mode prediction, modulated by a spatial coherence effect, was derived
based on the assumption of a gaussian line shape. The experimental
results were compared with this prediction and a high degree of
correlation between curve shapes was apparent. However, the effects
of multi-moding had reduced the amplitude of the experimental curve
significantly.

The results of this study can serve as a reference point for
improving the coherence of the laser by employing mode selection.
This should produce the greatest improvement in the area of temporal

coherence. Also the judicious placement of apertures and etalons in the laser cavity appear to be the most likely place to begin an experiment to improve the coherence properties of the laser.

THE COHERENCE PROPERTIES

OF A PULSED RUBY LASER

I. Introduction

The purpose of this study is to determine the coherence proper-
ties of a prospective holographic source, a pulsed ruby laser. These
properties are of interest because they limit the effectiveness of
the pulsed laser as a holographic source. A highly simplified intro-
duction to holography is presented to illustrate the potential of
this prospective source and to emphasize the need for the type of
analysis performed during this study.

Holography is a new method of forming optical images. It is
strikingly similar to photography in that they both record the effect
of the optical disturbance emanating from an object, but there is
a fundamental difference between the two. Photography is the
two-dimensional recording of an optical image on photographic emul-
sion. The optical disturbance proceeding from an object is trans-
formed by an optical system (camera) into the recorded image, whereas,
holography is the recording of the disturbance itself (photographic
emulsion is normally the recording medium). When the holographically
recorded disturbance is illuminated in a particular manner, a three
dimensional image is reconstructed which is identical to the original
object, as opposed to the two dimensional photographic likeness.

There are several arrangements used to record the optical
disturbance. Consequently, there are many types of holograms.
Although some of these arrangements are quite complex, they are all

variations of one general method. Described in simple terms, a beam
of laser light is divided into two components. One component (the
scene beam) illuminates the object, which transmits and reflects
portions of this illumination. Either the transmitted or reflected
portion is selected for recording. The second component of the source
beam (the reference beam) proceeds directly to the recording medium.
Mirrors are normally used to deflect the beams so that the optical
distance traversed by the two beams are identical. The scene and
reference beams meet at the recording medium and their interference
pattern is recorded. If both beams are stable during the duration of
the exposure, then spatial variations in intensity are recorded
(assuming that the recording medium is photographic emulsion). These
intensity variations are called interference fringes and the holo-
graphic arrangement is essentially an interferometer. When the
holographic record or "hologram" is illuminated with a beam similar
to the reference beam, the hologram transmits the beam with spatially
varying intensity due to the varying degrees of opacity of the holo-
gram. This complex transmitted wave contains the reconstructed image
of the original object as a component signal.

If the interference pattern is not stable for the duration of
the exposure, then the hologram will be seriously degraded (similar
to the blurred images caused by motion in photography). There are
two principal reasons why the interference pattern may be unstable.

The first reason is object motion. The logical solution to
this problem is to reduce the exposure time as the object motion
increases. However, to receive the same exposure, the intensity of

the laser source must increase as the exposure time decreases. The
pulsed ruby laser is very intense (when compared with continuous wave
gas lasers) and its one millisecond pulse duration is short for most
object motion. Thus the pulsed ruby laser warrants additional con-
sideration as a prospective source.

The second possible reason for an unstable interference pattern
is incoherent light. However, Stroke and Restrick have demonstrated
that quality holograms can be recorded, using a particular holographic
recording and reconstruction arrangement and spatially incoherent
light in the recording process (Ref 19). But, for most holographic
arrangements a coherent source is required to produce a perfect
hologram. In this context, a coherent source is a point source (no
finite physical size) of monochromatic (single-frequency) light.
These are obviously idealized conditions, and physical sources are
evaluated in terms of their departure from this ideal case, i.e.,
their degree of coherence. The degree of coherence is divided into
two categories, spatial and temporal coherence. The degree of spatial
coherence is a measure of the physical extent of the source and it
can be detected by considering the degree of phase correlation at two
different spatial points at any instant of time. The degree of
temporal coherence is a measure of the departure of the source from
monochromaticity.

Since the intensity and pulse duration of the pulsed ruby laser
do not limit its consideration as a prospective holographic source,
the analysis performed in this study is centered on the spatial and
temporal coherence properties of the laser.

The spatial and temporal coherence properties of a source do not exist independently. However some experimental arrangements tend to emphasize one more than the other. A form of Young's experiment was used in this study to effectively isolate spatial coherence effects. The experimental apparatus (a diffractometer) was similar to that used by Thompson and Wolf (Ref 21) in their measurement of the spatial coherence of a conventional source (the filtered yellow doublet of a mercury vapor lamp). However, some substitutions were made based on considerations of the intensity of the laser source and the availability of laboratory equipment.

The photographs of fringes resulting from the Young's experiment were analyzed with the aid of a densitometer and the relative intensities calculated using the Hurter-Driffield curves for the film. These experimental results were compared with a theoretical prediction based on a scalar wave analysis.

A Twyman-Green interferometer was used to isolate the temporal coherence effects. The interference fringes obtained were analyzed as before and the results compared with a theoretical prediction.

There are several allowable resonances or modes that may exist in the emitted radiation. These are determined largely by the laser cavity length and the average wave length of the emitted radiation. The actual emission may alternate between these allowed modes, or in the case of the ruby laser, may contain combinations of these modes. Thus the emitted radiation is actually a statistical phenomena. However, for normal holographic arrangements departures from single mode operation tend to seriously degrade the resulting hologram.

Consequently, the theoretical predictions were limited to single mode radiation.

Thus the pulsed ruby laser was analyzed as a prospective holographic source. In general, holography requires an intense, short duration, coherent source. The ruby laser satisfies the first two requirements. Consequently, it is the coherence properties that are of interest. These properties can be divided into spatial and temporal coherence properties.

Two experiments were chosen to isolate the spatial and temporal coherence effects. A modified Young's experiment was used to study spatial coherence and a Twyman-Green interferometer was used to study the temporal coherence properties. These experimental results were compared with a single-mode theoretical prediction.

Therefore, using these two experiments, the coherence properties of a multi-mode, pulsed, ruby laser were isolated, recorded, and analyzed. These results are presented in detail and in the same order that they have been introduced.

II. Measurement of Spatial Coherence

The spatial coherence properties were determined by using a modified version of Young's experiment. The time-averaged effect of the radiation was analyzed and compared with a theoretical prediction. This experiment will now be presented in the following sequence: description of equipment, experimental procedure, theory of operation, calculations, and discussion of results.

Description of Equipment

The equipment used to measure the spatial coherence was the laser source, a diffractometer, photographic film, a densitometer, and an X-Y recorder.

The Laser Source. The source was a pulsed laser which consisted of a Hughes Laboratory, Model 302 ruby laser, a pair of optical flats, an optical bench, and a laser power supply.

The ruby laser contained a ruby crystal (0.05% by weight Cr_2O_3 in Al_2O_3) in the form of a polished cylindrical rod with flat and parallel ends. The ends were also coated with a hard anti-reflecting film (MgF). The optic axis of the crystal rod was normal to the geometric axis of the rod. The crystal was three inches long with a diameter of 3/8 inches and it was mounted along the axis of a quartz, helical flash lamp. This lamp was filled with xenon gas and was designed for a maximum input energy of three thousand joules at four kilovolts.

The optical flats were made of hard glass and coated with a series of thin dielectric films. These coatings provided the output

REAR MIRROR 99%

23.4cm

24.7cm

18.4cm

RUBY CRYSTAL

FLASH LAMP

OUTPUT MIRROR 74%

FIGURE 1

THE LASER SOURCE
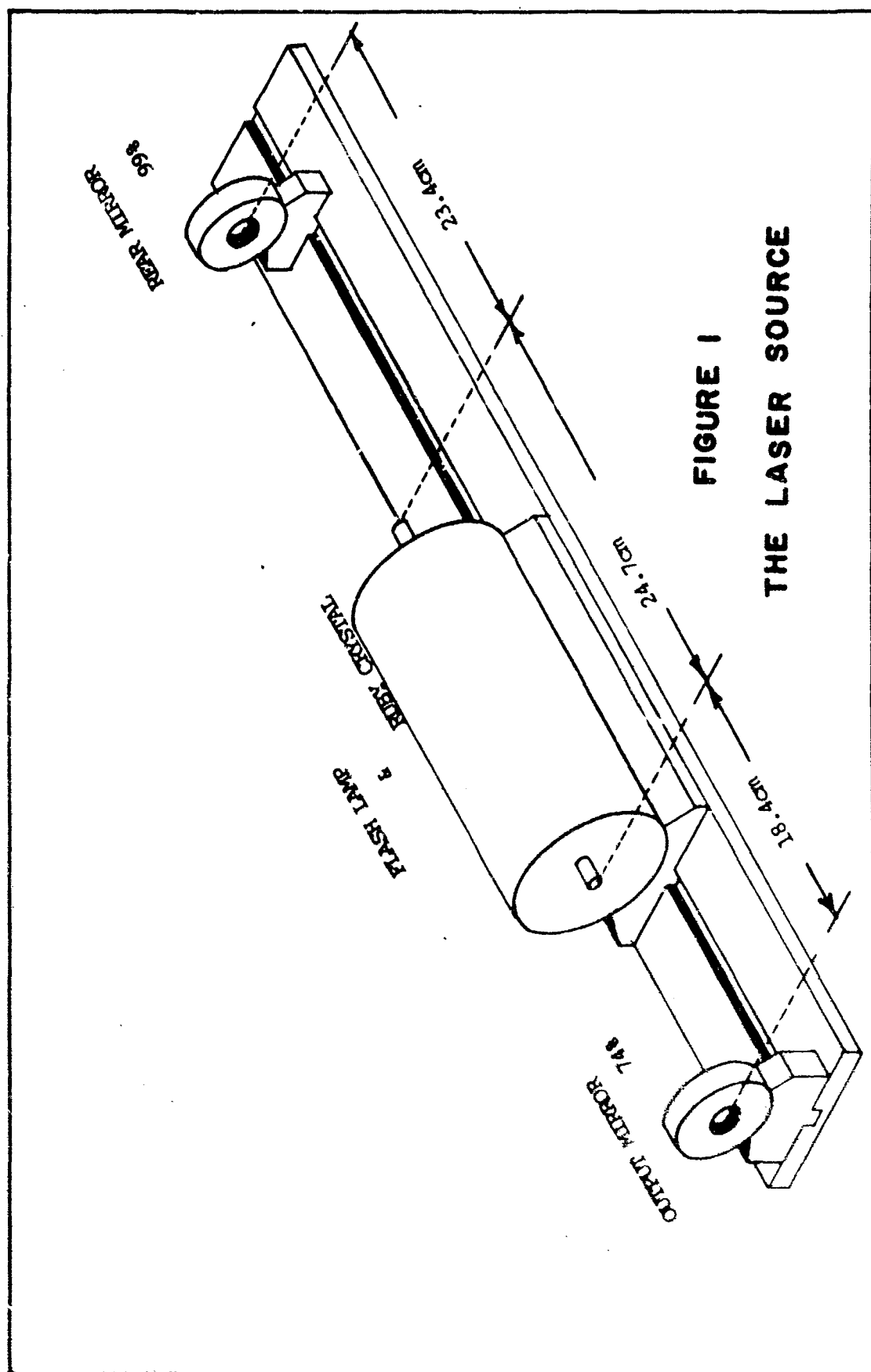
flat with a reflectivity of 74% and the opposite flat with a reflec-
tivity of 99%.

The length of the laser cavity was arbitrarily selected as shown
in Fig. 1.

The Diffractometer. The diffractometer consisted of a collima-
tion section, a screen, and an imaging section.

The collimation system consisted of a ten-power microscope
objective and a convex lens (L_2). The microscope objective was
corrected for coma and spherical aberration. The focal length of the
objective was approximately sixteen millimeters with a working dis-
tance of 7 millimeters (distance from the lens surface to the focal
point). The numerical aperture of the objective was 0.25. The lens
(L_2) was a 2.54 centimeter convex lens with a total thickness of
1.5 millimeters and a power of approximately 4.25 diopters.

The various screens were a set of 5.08 centimeter square aluminum
sheets, each 0.159 centimeters thick. Two circular apertures, with
diameters of 0.102 centimeters, were drilled into each sheet. The
separation of the holes was varied from one millimeter to nine milli-
meters in steps of 0.5 millimeters. Each pair of apertures was
centered on its respective screen.

The imaging section consisted of a lens (L_3), a microscope
objective, and a film plate (Kodak 103F, spectroscopic plate) placed
in the plane of best focus. The lens (L_3) and microscope objective
were identical to the lens and objective used in the collimation
section.

The dimensions of the diffractometer and the geometrical arrange-
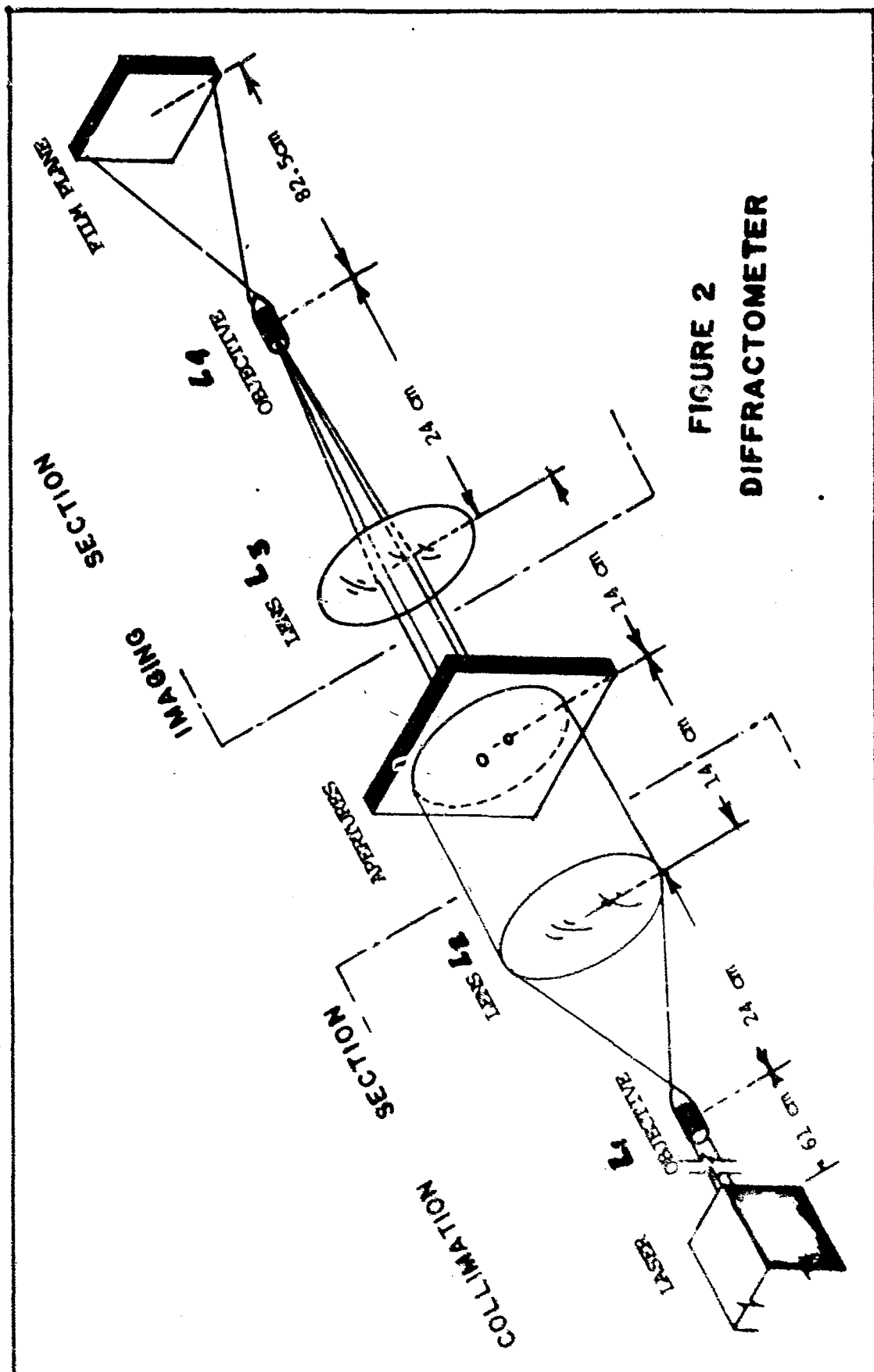ment of its three sections are shown in Fig. 2.

8

FIGURE 2
DIFFRACTOMETER

Experimental Procedure

The laser source was aligned with a helium-neon gas laser (0.6328 microns). The 99%-reflectance optical flat was placed on the bench first and aligned (centered on the helium-neon beam). The output mirror was placed on the bench next and aligned (centered on the beam and oriented to reduce off-axis reflections). Next the aluminum cylinder, containing the flash lamp and ruby crystal, was fastened to the bench, centered, and oriented for minimum off-axis reflections.

The alignment laser was then moved to the diffractometer to align its elements. When the elements were properly aligned, the far-field diffraction pattern of the circular aperture of the first microscope objective was imaged onto the film plane.

Then the laser source and diffractometer were aligned as a system by using the alignment laser to illuminate the diffractometer after the beam had passed through the laser cavity. The screens were placed in the diffractometer and centered so that the two apertures were approximately equally illuminated.

The capacitance of the energy storage bank in the laser power supply was set at 250 microfarads. The output voltage was set at 2.5 kilovolts corresponding to 781.5 joules of input energy. With the room in complete darkness, a Kodak 103F spectroscopic plate was placed behind a 0.3 neutral density filter in the film plane. Then the flash lamp was excited by pressing the manual trigger of the power supply. When the laser source was properly aligned, the ruby crystal lased and a diffraction pattern was recorded on the film plate. The laser was allowed a minimum of thirty minutes cooling time between shots.

10

The exposed plate was developed for 2 1/4 minutes in D-19 developer, held in short stop (to stop developing action) for approximately thirty seconds, and soaked for four minutes in fixer. The plate was then washed in cold running water for a minimum of one hour, bathed in photo-flow (to prevent water spotting during the drying process) for approximately fifteen seconds, and then allowed to dry.

The developed plate was cleaned with methanol (the side opposite the emulsion) and then placed on the densitometer. The densitometer, in conjunction with an X-Y recorder plotted the transmittance of the film relative to its fog level. The slit size and scan speed of the densitometer were set at the optimum position based on the condition of the plate, i.e., the sensitivity was increased and the scan speed was reduced as fringe contrast decreased. Also different neutral density filters were used to help increase the sensitivity of the densitometer when the fringe contrast was low.

The diffractometer screen was replaced by a screen with a different aperture separation and the preceding steps were repeated until approximately three good quality images were obtained for each aperture separation.

Theory of Operation

The use of the diffractometer casts this experiment into a form of Young's experiment, i.e., examining the far-field (Fraunhofer) diffraction pattern of two apertures when the apertures are illuminated by a plane wave.

The diffractometer was designed to accomplish this in the following manner. The laser radiation was a short pulse in the shape of

a beam of very small divergence (approximately ten milliradians) and approximately rectangular in cross-sectional shape. This beam was focused to a small spot by the microscope objective. The focused spot was located at the front focal point of the lens, L_2. An opaque screen containing a circular aperture, of diameter L_2 (not shown in Fig. 2), was placed in contact (the side nearest the front microscope objective) with L_2. Thus the collimating section produced a collimated beam 2.54 centimeters in diameter.

This beam was then incident on the two small apertures. Two collimated beams of diameter equal to the apertures emerged from the opposite side of the screen.

The two parallel beams were then collected by the lens, L_3, of the imaging section. The beams were brought together at the focal point of L_3 where interference occurred. The interference pattern, which was modulated by the degree of spatial coherence, was then imaged by the second microscope objective onto the film plane.

The film, containing the magnified version of the interference pattern, was developed and then scanned by the densitometer. The densitometer trace provided information concerning the relative densities (See Fig. 4) of the film. The relative intensities recorded were found by considering the Hurter-Driffield curves for the film which were provided by the manufacturer. This provided the information necessary to plot the visibility versus aperture separation curve (see graph I).

By representing the two microscope objectives as convex lenses having focal lengths of sixteen millimeters and several other
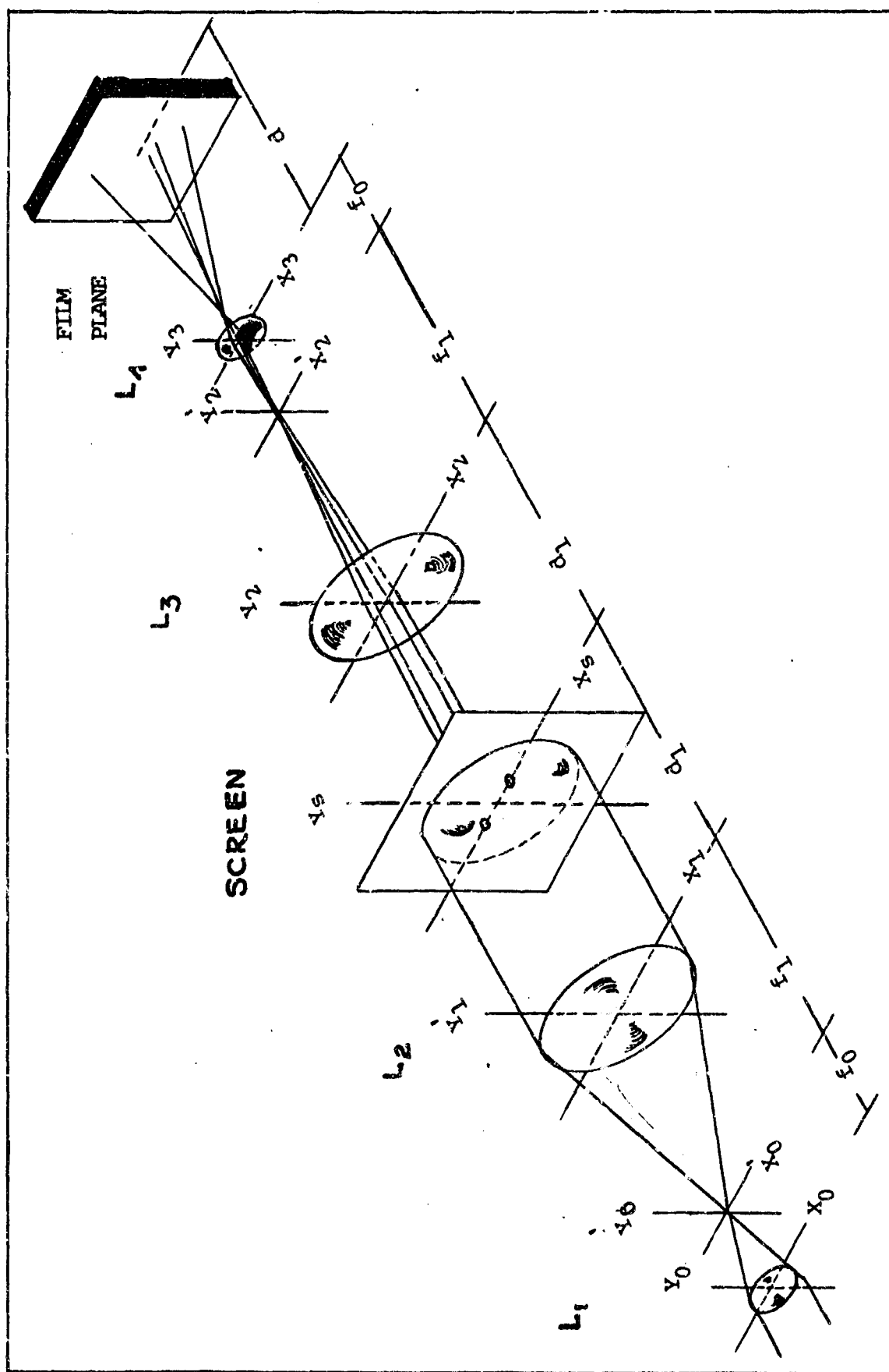
12

FIGURE 3
THEORETICAL MODEL

approximations, the preceding explanation can be examined more
rigorously. The method used is essentially the method suggested by
Goodman (Ref 8), i.e., the complex amplitude of the optical distur-
bance will be assumed to be a solution to the scalar wave equation.
The following theory will examine this theoretical model, as depicted
in Fig. 3, from left to right.

The laser radiation incident upon the diffractometer will be
assumed to be plane wave illumination. Also, the complex amplitude
will be assumed to be uniform across any cross-section. Thus the
complex amplitude incident on the microscope objective can be repre-
sented as

$$U(x_o, y_o) = A \; \text{RECT} \left(\frac{x_o}{L_x} \right) \text{RECT} \left(\frac{y_o}{L_y} \right) ,$$

$$\text{WHERE RECT } (x) = \begin{cases} 1, & |x| \leq 1/2 \\ 0, & \text{OTHERWISE} \end{cases} \qquad \text{(Ref 8:13)} \qquad (1)$$

and L_x and L_y are lengths in the x and y directions.

The finite beam has been replaced by an infinite plane wave illumi-
nating a small rectangular aperture in an infinite opaque screen.

Assuming that the geometrical cross-section of the incident beam
was smaller than the incident pupil of the microscope objective, the
illumination immediately behind the lens L_1 (model of microscope
objective), was the product of the incident amplitude and the ampli-
tude transmittance of the lens. The amplitude transmittance of a
positive lens has derived by Goodman and has been reproduced in the
following equation.

$$t(x,y) = e^{JKn\Delta_o} e^{-JK(x^2 + Y^2)/2f} \qquad \text{(Ref 8:80)} \qquad (2)$$

where the paraxial approximations are implicit. Also Δ_o is the physical thickness of the lens at its center, f_1 is the lens focal length, n_1 is the refractive index of the lens material, J is the square root of minus one, and K is the wave number. Therefore the complex amplitude of the disturbance immediately behind the lens L_1 is

$$U'(x_o,y_o) = A\, e^{JKn\Delta_o}\, e^{-\frac{JK}{2f_1}(x_o^2 + y_o^2)} \operatorname{RECT}\left(\frac{x_o}{L_x}\right) \operatorname{RECT}\left(\frac{y_o}{L_y}\right) \quad (3)$$

The Rayleigh-Sommerfeld diffraction formula (solution to the Hemholtz equation), becomes the Fresnel diffraction formula (Ref 8:60), if the distance Z is sufficiently large, i.e.

$$U(x_o,y_o) = \frac{e^{JKZ}}{J\lambda Z}\, e^{\frac{JK}{2Z}(x_o^2 + y_o^2)}\, \mathcal{F}\left\{U(x_1,y_1) e^{\frac{JK}{2Z}(x_1^2 + y_1^2)}\right\}\Bigg|_{\substack{f_x = \frac{x_o}{\lambda Z} \\ f_y = \frac{y_o}{\lambda Z}}} \quad (4)$$

where

$$\mathcal{F}\{g(x,y)\} = \int\!\!\!\int_{-\infty}^{\infty} g(x,y) e^{-2\pi J(f_x x + f_y y)}\, dx\, dy$$

and

$$\mathcal{F}^{-1} \{G(f_x, f_y)\} = \iint_{-\infty}^{\infty} G(f_x, f_y) \, e^{2\pi J(f_x x + f_y y)} \, df_x \, df_y \qquad (4)$$

form a Fourier transform pair.

The complex amplitude of the disturbance propagated a distance, f_o, to the (x_o', y_o')-plane. It can be described in this plane, by an application of the Fresnel diffraction formula, as $U(x_o', y_o')$, i.e.,

$$U(x_o', y_o') = \left(\frac{AL_x L_y}{J\lambda f_o}\right) e^{\frac{JK}{2f_o}(x_o'^2 + y_o'^2)} \, \text{SINC}\left(\frac{L_x x_o'}{\lambda f_o}\right) \, \text{SINC}\left(\frac{L_y y_o'}{\lambda f_o}\right) \qquad (5)$$

The constant phase factors will be ignored throughout the derivation since intensities are of ultimate interest. Sinc(x) is defined as

$$\text{SINC}(x) = \text{SIN}(\pi x)/\pi x \qquad (\text{Ref } 8:14)$$

After propagating a distance, f_1, the complex amplitude in the (x_1, y_1)-plane can be described by another application of the Fresnel diffraction formula.

Let

$$g(x_o', y_o') = e^{J\frac{a}{2}(x_o'^2 + y_o'^2)} \, \text{SINC}(bx_o') \, \text{SINC}(cy_o') \qquad (6)$$

16

where

$$a = K \left(\frac{1}{f_o} + \frac{1}{f_1} \right) , \quad b = \frac{L_x}{\lambda f_o} , \quad \text{AND} \quad c = \frac{L_y}{\lambda f_o} \qquad (6)$$

By using the zero order Hankel Transform,

$$B \{g(r)\} = 2\pi \int_0^\infty r g(r) J_o(2\pi r \rho) dr,$$

it can be shown that

$$G(f_x, f_y) = \frac{J}{abc} e^{-J \frac{(2\pi\rho)^2}{2a}} * \left[\text{RECT} \left(\frac{f_x}{b} \right) \text{RECT} \left(\frac{f_y}{c} \right) \right]$$

where $G(f_x, f_y) = \mathscr{F}\{g(x_o', y_o')\}$ and the symbol, *, implies the convolution, i.e.,

$$g(x,y) * h(x,y) = \iint_{-\infty}^\infty g(\xi, n) h(x-\xi, y-n) d\xi dn \qquad (7)$$

Therefore, after a change of variables and some rearrangement of the convolution integral, $G(f_x, f_y)$ becomes

$$G(f_x, f_y) = \frac{J}{4\pi bc} \left(\int_{\alpha_1}^{\alpha_2} e^{-J \frac{\pi}{2} U^2} du \right) \left(\int_{\beta_1}^{\beta_2} e^{-J \frac{\pi}{2} v^2} dv \right),$$

17

where

$$\alpha_1 = 2\sqrt{\frac{\pi}{a}}\left(f_x - \frac{b}{2}\right) \qquad \beta_1 = 2\sqrt{\frac{\pi}{a}}\left(f_y - \frac{c}{2}\right)$$

$$\alpha_2 = 2\sqrt{\frac{\pi}{a}}\left(f_x + \frac{b}{2}\right) \qquad \beta_2 = 2\sqrt{\frac{\pi}{a}}\left(f_y + \frac{c}{2}\right) \qquad (8)$$

The integrals in this equation can be interpreted in terms of the Fresnel integrals (Ref 8:71) and

$$G(f_x, f_y) = \frac{J}{4\pi bc}\left\{[c(\alpha_2) - c(\alpha_1)] + J[S(\alpha_2) - S(\alpha_1)]\right.$$

$$\left.[c(\beta_2) - c(\beta_1)] + J[S(\beta_2) - S(\beta_1)]\right\}$$

where

$$c(\alpha) = \int_0^\alpha \cos\left(\frac{\pi t^2}{2}\right) dt \quad \text{AND} \quad S(\alpha) = \int_0^\alpha \sin\left(\frac{\pi t^2}{2}\right) dt. \qquad (9)$$

This equation can be evaluated with the aid of the Cornu spiral. First consider α_1, α_2, β_1 and β_2, when $f_x = \frac{x_1}{\lambda f_1}$, $f_y = \frac{y_1}{\lambda f_1}$, $f_1 = 23.5$ centimeters, $f_o = 1.6$ centimeters, and $\lambda = 0.6943$ microns. Then it follows that

$$x_1 > \frac{L_x f_1}{2f_o} \rightarrow c(\alpha_1) = S(\alpha_1) = \frac{1}{2}$$

$$x_1 < \frac{L_x f_1}{2f_o} \rightarrow c(\alpha_1) = S(\alpha_1) = -\frac{1}{2}$$

$$x_1 > \frac{L_x f_1}{2f_o} \rightarrow c(\alpha_2) = S(\alpha_2) = -\frac{1}{2}$$

$$x_1 < -\frac{L_x f_1}{2f_o} \rightarrow c(\alpha_2) = S(\alpha_2) = \frac{1}{2} \tag{10}$$

Similar results can be shown for y_1, and $\frac{L_y f_1}{2f_o}$, and $c(\beta_1)$, $c(\beta_2)$, $S(\beta_1)$, and $S(\beta_2)$. Therefore Eq (9) becomes

$$G(f_x, f_y) \Big|_{\substack{f_x = \frac{x_1}{\lambda f_1} \\ f_y = \frac{y_1}{\lambda f_1}}} = -\frac{\lambda^2 f_o^2}{2\pi L_x L_y} \text{RECT} \left(\frac{f_o x_1}{L_x f_1} \right) \text{RECT} \left(\frac{f_o y_1}{L_x f_1} \right) \tag{11}$$

The Fresnel diffraction formula could finally be applied so that the complex amplitude in the (x_1, y_1)-plane was

$$U(x_1, y_1) = \left(\frac{\lambda f_o}{2\pi f_1} \right) e^{\frac{JK}{2f_1}(x_1^2 + y_1^2)} \text{RECT} \left(\frac{f_o x_1}{L_x f_1} \right) \text{RECT} \left(\frac{f_o y_1}{L_x f_1} \right) \tag{12}$$

19

The complex amplitude $U(x_1,y_1)$ represented the disturbance incident on the lens L_2. The complex amplitude immediately behind L_2 was

$$U'(x_1,y_1) = U(x_1,y_1)t_{L2}(x_1,y_1)P_2(x_1,y_1) \qquad \text{(Ref 8:83)}$$

$$U'(x_1,y_1) = \frac{Af_o}{2\pi f_1} e^{\frac{JK}{2f_k}(x_1^2 + y_1^2)} \left[RECT\left(\frac{x_1 f_o}{L_x f_1}\right)\right.$$

$$\left. RECT\left(\frac{y_1 f_o}{L_y f_1}\right)\right] e^{-\frac{JK}{2f_1}(x_1^2 + y_1^2)} CIRC\left(\frac{\sqrt{x_1^2 + y_1^2}}{L_{r2}}\right) \qquad (13)$$

where f_1 = focal length of L_2 and L_{r2} = radius of L_2.

Thus the illumination leaving L_2 was constant in amplitude and phase. Considering the values of f_o, f_1, L_x, and L_y, the area of the rectangular pulse in this plane was approximately 1.2 centimeters x 2.8 centimeters. The diameter of the lens was 2.54 centimeters. Therefore the geometrical shape of $U'(x_1,y_1)$ was rectangular with rounded ends in the $\pm y_1$-directions.

The restriction of the rect function, $RECT\left(\frac{y_1 f_o}{L_y f_1}\right)$, imposed by the pupil function of the lens ($circ\left(\frac{r_1}{L_{r2}}\right)$), could be approximated by a smaller rect function. Thus $U'(x_1,y_1)$ became

20

$$U'(x_1, y_1) = \frac{Af_0}{2\pi f_1} \text{RECT} \left(\frac{x_1 f_0}{L_x f_1} \right) \text{RECT} \left(\frac{y_1}{L_{r2}} \right) \tag{14}$$

Assuming propagation from the (x_1, y_1)-plane to the (x_s, y_s)-plane (a distance d_1) was deep within the Fresnel region, $U(x_s, y_s)$ can be determined by another application of the Fresnel diffraction formula. Whenever $\lambda \ll \frac{1}{100Z}$, propagation can be assumed to be deep within the Fresnel diffraction region. Goodman has performed this calculation (Ref 8:71) and

$$U(x_s, y_s) = \frac{Af_0}{2\pi f_1} \text{RECT} \left(\frac{x_s f_0}{L_x f_1} \right) \text{RECT} \left(\frac{y_s}{L_{r2}} \right) \tag{15}$$

Thus $U(x_s, y_s)$ is the geometrical projection of $U'(x_1, y_1)$.

The amplitude transmittance of the screen was

$$t_s(x_s, y_s) = \text{CIRC} \left(\frac{\sqrt{(x_s - h)^2 + y_s^2}}{L_{rs}} \right) + \text{CIRC} \left(\frac{\sqrt{(x_s + h)^2 + y_s^2}}{L_{rs}} \right) \tag{16}$$

where $\pm h$ was the distance to the center of the respective aperture and L_{rs} was the radius of the aperture. The complex amplitude immediately behind the screen was $U'(x_s, y_s) = U(x_s, y_s) t(x_s, y_s)$. Considering the areas affected by the geometry of $U'(x_s, y_s)$, i.e., the rect functions represented a rectangular spot size of approximately 1.2 centimeters x 2.5 centimeters. The diameter of each aperture was approximately one millimeter with a maximum separation of nine

21

millimeters between the centers of the two apertures. Consequently, $U'(x_s, y_s)$ could be further approximated as

$$U'(x_s, y_s) = \frac{Af_o}{2\pi f_1} \left[CIRC \left(\frac{\sqrt{(x_s-h)^2 + y_s^2}}{L_{rs}} \right) + CIRC \left(\frac{\sqrt{(x_s+h)^2 + y_s^2}}{L_{rs}} \right) \right] \tag{17}$$

Assuming that the propagation of the disturbance was still deep in the Fresnel region, $U(x_2, y_2)$ is the geometrical projection of $U'(x_s, y_s)$, i.e.,

$$U(x_2, y_2) = \frac{Af_o}{2\pi f_1} \left[CIRC \left(\frac{\sqrt{(x_2-h)^2 + y_2^2}}{L_{rs}} \right) + CIRC \left(\frac{\sqrt{(x_2+h)^2 + y_2^2}}{L_{rs}} \right) \right] \tag{18}$$

The complex amplitude immediately behind the lens, L_3, was $U'(x_2, y_2)$, where $CIRC \left(\frac{r_2}{L_{r3}} \right) = 1$ when the area illuminated by $U(x_2, y_2)$ is considered. Thus

$$U'(x_2, y_2) = U(x_2, y_2) e^{-\frac{JK}{2f_1}(x_2^2 + y_2^2)} \tag{19}$$

22

The disturbance propagated a distance, f_1, to the (x_2', y_2')-plane. The complex amplitude in this plane was determined by another application of the Fresnel diffraction formula and

$$U(x_2', y_2') = \frac{A f_o}{J \pi f_1} e^{\frac{JK(r_2')^2}{2f_1}} \left[\cos\left(\frac{Khx_2'}{f_1}\right)\right] \left[\frac{J_1\left(\frac{KL_{rs} r_2'}{f_1}\right)}{r_2'}\right] \qquad (20)$$

Geometrical optics was assumed for the imaging of the complex amplitude, $U(x_2', y_2')$, onto the film plane (x,y). This assumption yields a simple relation between the object and image amplitude distributions, i.e.,

$$U_1(x,y) = \frac{1}{M} U_o\left(\frac{-x}{M}, \frac{-y}{M}\right) \qquad \text{(Ref 8:96)} \qquad (21)$$

where U_1 = complex amplitude of the image,

U_o = complex amplitude of the object,

and M = magnification.

Thus the complex amplitude in the image plane (film plane) was

$$U(x,y) = \frac{Ad}{J \pi f_1} e^{\frac{JK}{2f_1}\left(\frac{f_o r}{d}\right)^2} \left[\cos\left(\frac{Khf_o x}{df_1}\right)\right] \left[\frac{J_1\left(\frac{KL_{rs} f_o r}{df_1}\right)}{r}\right] \qquad (22)$$

The intensity in the film plane was

23

$$I(x,y) = \left(\frac{Ad}{J\pi f_1}\right)^2 \left[\cos^2\left(\frac{Khf_o x}{df_1}\right)\right] \left[\frac{J_1^2\left(\frac{KL_{rs}f_o r}{df_1}\right)}{r^2}\right] \quad (23)$$

Consider a quasi-monochromatic source whose complex amplitude is represented by $U(x_o, y_o)$. Then each point of the source will produce coherent illumination in the (x_o', y_o')-plane. Assuming that the image of the source (the sum of the Fraunhofer diffraction patterns of each source point, which may be added incoherently) is much larger than the diffraction pattern of a typical source point, then the disturbance $U(x_o', y_o')$ may be interpreted as resulting from a secondary incoherent source (σ).

This assumption allows the Van Cittert-Zernike theorem to be invoked (Ref 3:509). If $|\gamma_{12}(\tau)|$ = the magnitude of complex degree of spatial coherence, then $\gamma_{12}(\tau) \simeq \gamma_{12}(0)$

where $\tau = \dfrac{R_2 - R_1}{C}$

and

$$\gamma_{12}(0) \simeq \frac{1}{[I(P_1)I(P_2)]^{1/2}} \int_\sigma \frac{I(\sigma)\, e^{JK(R_1 - R_2)}}{R_1 R_2}\, d\sigma \quad (24)$$

$I(\sigma)$ is the intensity, per unit area, of the source. Also the assumption $|\tau| \ll \dfrac{1}{\Delta\nu}$, is implicit in these approximations.

The intensity of the secondary source had $\left(\dfrac{AL_x L_y}{\lambda f_o}\right)^2$ as the intensity of its central spot. The size of this spot (S_o) was

24

$$S_o \simeq \theta F \qquad \text{(Ref 6:1)}$$

where θ = beam divergence angle and F = focal length of lens used.
Then due to the small separation of the apertures, the intensity of
the central spot was a good approximation to that part of the source
which illuminated the apertures or

$$I(\sigma) = \left(\frac{AL_x L_y}{\lambda f_o} \right)^2 \text{RECT}^2 \left(\frac{x_o'}{\theta f_o} \right) \text{RECT}^2 \left(\frac{y_o}{2\theta f_o} \right) \qquad (25)$$

Since the apertures were symmetrically located along the x_1-axis,
then R_1 & R_2 (distances from a source point to the center of the
respective aperture) were

$$R_1 = [(h - x_o')^2 + y_o'^2 + f_1^2]^{1/2} \quad \text{AND} \quad R_2 = [(h + x_o')^2 +$$

$$y_o'^2 + f_1^2]^{1/2}$$

If the apertures were equally illuminated, then $I(P_1) = I(P_2)$
$= I(P)$.

Equation (24) becomes:

$$I(P) \simeq 2 \left(\frac{AL_x L_y \theta}{\lambda f_1} \right)^2$$

25

and

$$\gamma_{12}(0) \approx \frac{1}{I(P)} \int_\sigma \frac{I(\sigma) \, e^{JK(R_1 - R_2)}}{R^2} \, d\sigma$$

$$\gamma_{12}'(0) \approx SINC \left(\frac{\theta f_o h}{\bar{\lambda} f_1} \right) \tag{26}$$

where $\theta = 10^{-2}$ radians (Hughes specifications), $f_o = 16 \times 10^{-3}$ m, $f_1 = 23.55$ cm, and $\bar{\lambda} = 6.943 \times 10^{-7}$ m.

The preceding derivation began with monochromatic light (through Eq (23)) and was then generalized to quasi-monochromatic light

$$|\tau| = \left| \frac{X_2 - R_1}{c} \right| \ll \frac{1}{\Delta\nu} \quad . \quad \text{Born and Wolf illustrated that the}$$

quasi-monochromatic intensity $(I(Q))$ at a point Q, in the film plane is given by (Ref 3:502)

$$I(Q) = I^{(1)}(Q) + I^{(2)}(Q) + \left\{ 2[I^{(1)}(Q)I^{(2)}(Q)]^{1/2} |\gamma_{12}(\tau)| \right.$$

$$\left. COS \left[\phi(\tau) - K(S_2 - S_1) \right] \right\} \tag{27}$$

Continuing the assumption of equal illumination of the apertures, Eq (23) becomes

$$I(r) = \left(\frac{Ad}{\pi f_1}\right)^2 \left[\frac{J_1^2\left(\frac{KL_{rs}f_o r}{df_1}\right)}{2r^2}\right]\left[1 + \right.$$

$$\left. \left| \text{SINC}\left(\frac{\theta f_o h}{\bar{\lambda}f_1}\right) \right| \cos\left(\frac{2hxf_o K}{df_1}\right)\right] \qquad (28)$$

This intensity distribution was demonstrated by the fringes recorded. These fringes are depicted in Fig. 4.

Thus the fringes observed in the film plane had maxima for $x = \frac{2n\pi df_1}{2hf_o}$ and minima for $x = \frac{(2n+1)\pi df_1}{2hf_o}$, n=0,1,2... . The fringe contrast was determined by the function $\text{sinc}\left(\frac{\theta f_o 2h}{2\bar{\lambda}f_1}\right)$. This function experiences maxima and minima given by the following relations:

$\text{Sinc}\left(\frac{2h\theta f_o}{2\bar{\lambda}f_1}\right)$ is a maximum for $\frac{\theta 2hf_o}{2\bar{\lambda}f_1}$ such that

$$\tan\left(\frac{\theta f_o 2h}{2\bar{\lambda}f_o}\right) = \frac{\theta f_o 2h}{2\bar{\lambda}f_1} \qquad \text{(Ref 3:394)}$$

$\text{Sinc}\left(\frac{\theta f_o 2h}{2\bar{\lambda}f_1}\right) = 0$, for $2h = \frac{2n\bar{\lambda}f_1}{\theta f_o}$, n=1,2,... .

27

0.3 Neutral Density Filter

2¼ Minute Developement Time

(a) 1mm Separation
1.2mm x3microns Slit Size
1mm/min Scan Speed

(b) 2mm Separation
0.5mm x3microns Slit Size
0.5mm/min

(c) 3mm Separation
1.2mm x3microns Slit
Size
1mm/min Scan Speed
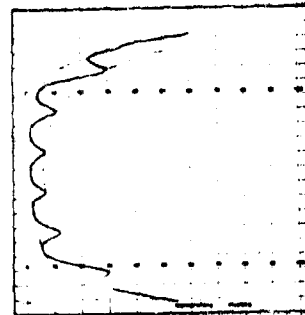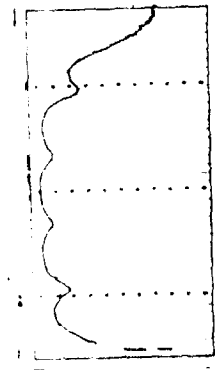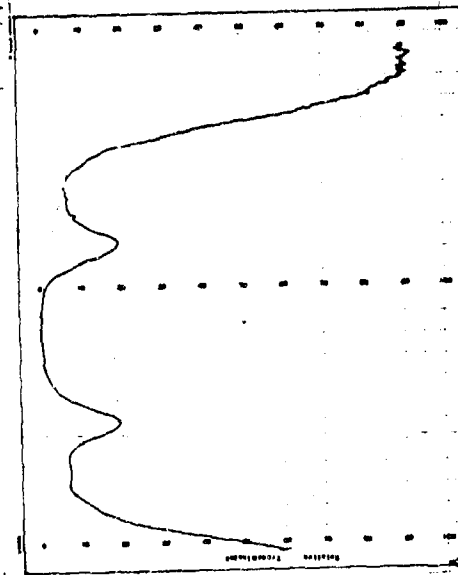
FIGURE 4

TYPICAL   INTERFERENCE   FRINGES   &   DENSITOMETER   TRACES   FOR   SPATIAL   COHERENCE

28

(d) 4 mm Separation
1.2 mm x 3 microns Slit Size
1 mm/min Scan speed
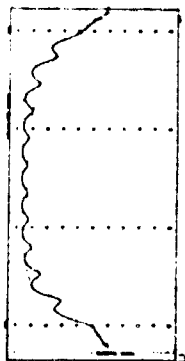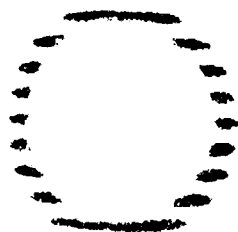
(e) 5 mm Separation
1.2 mm x 1 micron Slit Size
0.5 mm/min Scan Speed
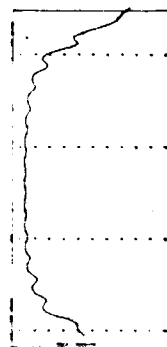
(f) 6 mm Separation
1.2 mm x 1 micron Slit Size
0.5 mm/min Scan Speed

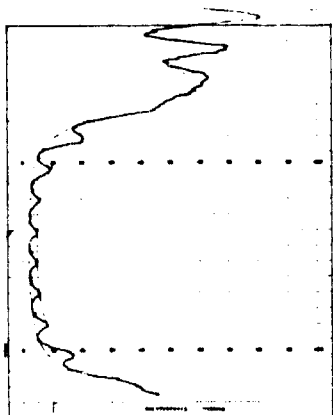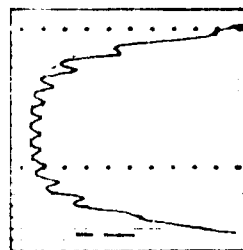(g) 7 mm Separation
1.2 x 3 microns Slit Size
1 mm/min Scan Speed

29

The visibility (V) of the fringes is defined as

$$V = \frac{I_{max} - I_{min}}{I_{max} + I_{min}} \tag{29}$$

Thus using Eq (28)

$$V = \left| SINC \left(\frac{\theta f_o^2 h}{2\bar{\lambda} f_1} \right) \right| = |\gamma_{12}(0)| \tag{30}$$

Should the assumption of equal illumination of the apertures prove to
be unjustified, then Eq (27), should be used, i.e.

$$V = \frac{2\sqrt{I^{(1)}(Q)I^{(2)}(Q)}}{I^{(1)}(Q) + I^{(2)}(Q)} |\gamma(0)| \tag{31}$$

The fact that the laser pulse contains several modes, some
simultaneously, during each pulse leads to the next generalization of
the optical disturbance. An analysis of each mode shows that each
satisfies the requirement for quasi-monochromatic illumination. Thus
photographic film exposed for the duration of the pulse, will exhibit
the integrated intensity of all modes and measure the statistical
average coherence effect of the individual modes. Pursuing this line
of reasoning, Chang and Gray formulated the following expression
(Ref 4:50):

$$V = \frac{2\left|\sum_J [I_J^{(1)}(Q)I_J^{(2)}(Q)]^{1/2}\ \gamma_{J_{12}}(\tau)e^{J\xi_J}\right|}{\sum_J I_J^{(1)}(Q) + \sum_J I_J^{(2)}(Q)} \tag{32}$$

where the subscript J refers to the Jth mode.

In this experiment the film contrast was evaluated using a densitometer whose output was recorded using an X-Y recorder. The densitometer and the film represent an incoherent optical system. Assuming the film to be used in the linear region of the Hurter-Driffield curve (see Fig. 5), we can write the following relation.

$$D = \gamma\ LOG_{10}\ E - D_o \tag{33}$$

where D is photographic density, E is exposure, and γ is the slope of the H-D curve.

If the definitions $D = LOG_{10}\left(\frac{1}{\tau}\right)$ and $E = IT$, (where τ = local average $\left(\frac{I\ transmitted}{I\ incident}\right)$, I = exposing intensity, and T = exposure time (duration of laser pulse), are used, then it follows that

$$I = K(\tau)^{-\frac{1}{\gamma}},\ where\ K = \left(\frac{1}{T}\right)10^{\frac{D_o}{\gamma}} \tag{34}$$

Equation (29) becomes

$$V = \frac{(\tau_{min})^{-\frac{1}{\gamma}} - (\tau_{max})^{-\frac{1}{\gamma}}}{(\tau_{min})^{-\frac{1}{\gamma}} + (\tau_{max})^{-\frac{1}{\gamma}}} \tag{35}$$

FIGURE 5

HURTER – DRIFFIELD CURVES FOR KODAK 103F, SPECTROSCOPIC PLATES

This would be an accurate measure of the visibility had the film
been exposed by incoherent light. However, the film had been exposed
by individual modes which have been shown to be spatially coherent
(Ref 5:1409). When a transparency has been exposed by coherent
radiation, it can be described in terms of an amplitude transmittance
(t), where $t = c |U|^{-\gamma}$. Here c, is a constant and U, is the complex
amplitude exposing the film (Ref 8:155). Thus the densitometer
provides a mapping of coherent amplitude information from one source
(neglecting phase variations) recorded on the film into incoherent
intensity information from another source, i.e., $t_{s1} = \phi \tau_{s2}$, where
ϕ is some linear transformation imposed by the densitometer.
Theoretically, ϕ could be determined by evaluating film with known
values of t_{s1} and obtaining τ_{s2} from the densitometer output. Then
Eq (35) becomes

$$V' = \frac{(t_{min})^{-\frac{1}{\gamma}} - (t_{max})^{-\frac{1}{\gamma}}}{(t_{min})^{-\frac{1}{\gamma}} + (t_{max})^{-\frac{1}{\gamma}}} \tag{36}$$

Some typical densitometer traces are shown in Fig. 4.

Since coherent light is not linear in intensity, a good measure
of the visibility is $V = (V')^2$ where amplitude phase variations have
been neglected. This approach yields results that agree favorably
with those predicted by Eqs (28) and (36) (see graph I).

Calculations

An envelope of the fringe maxima and another of the minima were constructed on each graph produced by the densitometer-recorder system. The value of the maximum envelope (τ_{min}) and the corresponding minimum (τ_{max}) at the center of the fringe pattern were obtained.

The values of the maximum and minimum densities of each plate were calculated using the relation

$$D = \text{Log}_{10}\left(\frac{1}{\tau}\right) = 0.43429\text{Ln}\left(\frac{1}{\tau}\right) .$$

The Olivetti Programma 101, computer-calculator, was used to perform these calculations.

The calculated densities were used in conjunction with the Hurter-Driffield (H-D) curves to determine the slope (γ) of the curve corresponding to the maximum and minimum densities of each plate. The slope of the secant line connecting the two points of the curve (D_{min} and D_{max}) was the value used for gamma when $0.5 \leq D_{min} < D_{max} \leq 2$, i.e., when the two points lay on the linear portion of the curve. For points that lay outside of this range, the slope of the H-D curve at each of the two points was determined.

Once the gammas were known, the visibility of each plate was determined. For densities lying within the linear region of the H-D curve, the relation

$$V = \frac{(\tau_{min})^{-\frac{1}{\gamma}} - (\tau_{max})^{-\frac{1}{\gamma}}}{(\tau_{min})^{-\frac{1}{\gamma}} + (\tau_{max})^{-\frac{1}{\gamma}}} \qquad \text{was used.}$$
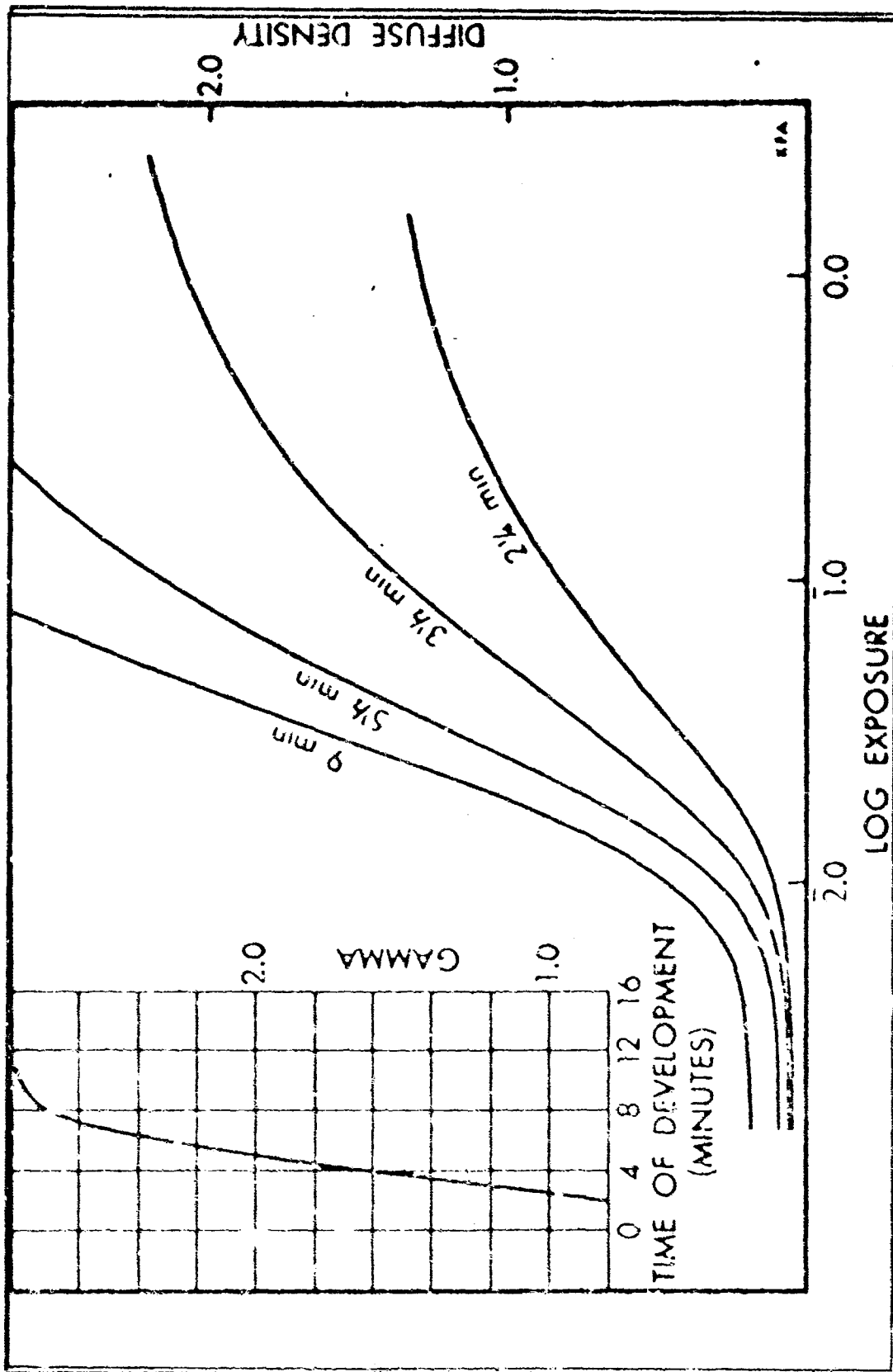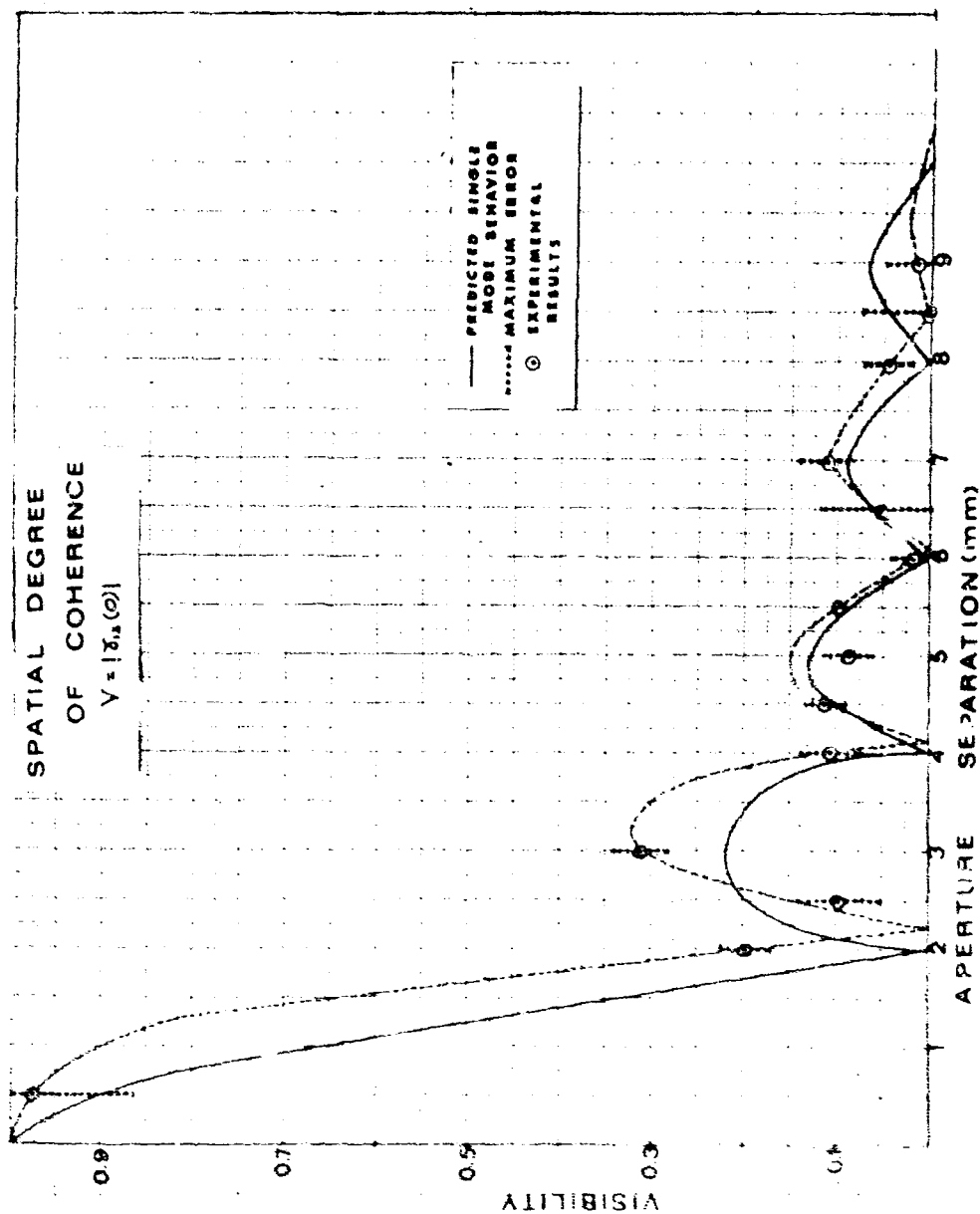
GRAPH I - DEGREE OF SPATIAL COHERENCE

For densities lying outside of this region the visibility was calculated using

$$V = \frac{(\tau_{min})^{-\frac{1}{\gamma_{min}}} - (\tau_{max})^{-\frac{2}{\gamma_{max}}}}{(\tau_{min})^{-\frac{1}{\gamma_{min}}} + (\tau_{max})^{-\frac{1}{\gamma_{max}}}}$$

Each value of the visibility was then squared and plotted as a function of aperture separation. The visibility was also calculated using the gamma (1.12) extracted from the graph of gamma as a function of development time. These calculations are summarized in graph I and table I, where arithmetic average of the three visibility values and the three gammas for each plate are exhibited.

Discussion of Results

No mode control or mode selection was employed during this experiment, with the exception of that imposed by the cavity length, physical size and radius of curvature of the two optical flats, and the constant input energy used to excite the flash lamp. Consequently, it was possible for the instantaneous emission to contain simultaneous, spatially separated transverse modes which could interfere, with the magnitude of this effect depending on the extent of the spatial separation (phase difference) of the modes. Also randomly spaced transverse modes could have been emitted at different times during the pulse in a statistical manner. Thus the time averaged effect for one long pulse should exhibit a statistical variation among other long pulses for a particular experimental environment.

This explains the difference between the single transverse mode predicted curve and the actual curve obtained. To accurately predict the experimental curve, the time averaged spot size and shape in the focal plane of the first microscope objective should be known. As an alternative, an approximate model of the lasing radiation (time-averaged effect) could be constructed by the addition of transverse modes with carefully chosen phase differences. This method would require the existence of the experimental curve. Then (with the aid of a computer) as a transverse mode is added, the resulting theoretical visibility curve could be compared with the experimental curve until the desired accuracy was obtained. Due to the small path difference of the illumination from the two aperture the effect of multiple longitudinal modes in the plane of the film was negligible.

It was mentioned above that each point of the visibility curve should represent a statistical distribution. The fact that an average of only three shots per separation was utilized implies the existence of a degree of uncertainty connected with each point. A consideration of this uncertainty will be considered next.

An examination of the maximum error possible in the calculation of visibility (V) might begin with the uncertainty associated with the determination of the gamma (slope of the Hurter-Driffield Curve) values. A measure of this uncertainty can be obtained by determining the gamma value from the gamma as a function of development time curve, calculating the visibility using this gamma, and then comparing the result with the visibility calculation using the gamma from the H-D curve. Then the maximum error in visibility due to an uncertainty in

the gamma determination is

$$\Delta V_\gamma = (V'_{\gamma,H-D})^2 - (V'_{\gamma,*})^2 \tag{37}$$

Here $V'_{\gamma,H-D}$ and $V'_{\gamma,*}$ are the amplitude visibility functions calculated using the two gamma values. Since the H-D curves relate density and exposure, determinations of gamma fror these curves will have inaccuracies based on the accuracy of the measurements of the transmittances of the film. However, the maximum error in visibility due to an error in the determination of the amplitude transmittance will be considered next. Consequently, to include this inaccuracy with error due to the uncertainty in gamma would be an unrealistic magnification of the actual error.

Now consider the maximum error in the intensity visibility due to an uncertainty in the amplitude transmittance of the film. First the amplitude visibility is given by Eq (36). Next the maximum error in the amplitude visibility is given by

$$\Delta V' = \frac{\partial V'}{\partial t_1} \Delta t_1 + \frac{\partial V'}{\partial t_2} \Delta t_2 \tag{38}$$

There are two sources of error in the determination of the transmittance. First, the density of the unexposed film was not uniform. Next the response of the densitometer-recorder combination limits the transmittance accuracy. The magnitude of error introduced by the nonuniformity of film density is probably random. In any case, there is irsufficient information upon which to base an estimate of the

38

error introduced. The latter source of error would be of the same magnitude for both transmittances, i.e., $|\Delta t_1| = |\Delta t_2| = |\Delta t|$. Thus the maximum error in the amplitude transmittance becomes

$$\Delta V_t' = \frac{\frac{2\Delta t}{\gamma}\left(\frac{1}{t_1}+\frac{1}{t_2}\right)}{\left[\left(\frac{t_1}{t_2}\right)^{-\frac{1}{2\gamma}}+\left(\frac{t_2}{t_1}\right)^{-\frac{1}{2\gamma}}\right]^2} \qquad (39)$$

Then the maximum error in the intensity visibility becomes

$$\Delta V_t = 2V'\Delta V_t' + (\Delta V_t')^2 \qquad (40)$$

The spread in visibility values for each point also represents an uncertainty. This precision factor was added to the total maximum error and

$$\Delta V_{max} = \Delta V_\gamma + \Delta V_t + \Delta V_p \qquad (41)$$

In addition to the non-uniform film density, there were other sources of possible error that were not considered because of the difficulty in estimating the maximum error in visibility that they could introduce.

First the laser was cooled by radiation into a room temperature reservoir rather than by convection into water, liquid nitrogen, or some other more efficient means. Also the laser was not fired at constant time intervals. Consequently, it was possible for the

crystal to be at different points on its cooling curve at the time of each shot.

Next the film was exposed in complete darkness which caused a time delay in placing the unexposed film into its holder and navigating around the room to the laser power supply to fire the laser. If the energy storage network had not stabilized, then the excitation voltage might be more than the constant value assumed.

Equation (31) suggests another source of error, non-uniform illumination. The amplitude analog of this effect is

$$V' = \frac{2(|U^{(1)}||U^{(2)}|)^{1/2} |\gamma(0)|^{1/2}}{|U^{(1)}| + |U^{(2)}|} \tag{42}$$

To consider the magnitude of the error introduced by non-uniform illumination, let

$$|U^{(1)}| = K|U^{(2)}|, \ K \geq 1$$

Then consider the fractional change in the visibility (intensity) when compared with visibility arising from uniform illumination, i.e.

$$\frac{V_k}{V} = 4 \frac{K}{(K + 1)^2} \tag{43}$$

Here V, represents the intensity visibility function for uniform illumination and V_k, the corresponding function for non-uniform illumination. This fractional error can not be estimated without a knowledge of the ratios of the complex amplitudes for each aperture

separation. However, the fractional error involved may be considered negligible for most applications. For example, a value of K equal to 1.414 would reduce the visibility to only 0.97 of its uniform illumination value. This particular value of K is an extremely conservative figure since it represents an intensity ratio of two.

An examination of Fig. 4 reveals an asymmetry of the fringe patterns (most noticeable on the densitometer traces). This implies a misalignment of the source and the two apertures. It can be shown that this can result in a reduction of fringe visibility (Ref 16:9).

The effects of misalignment and non-uniform illumination increase with aperture separation. Increasing separation would increase the angle of misalignment for one aperture and decrease the angle for the other, thus resulting in more asymmetry in the film plane and an increasing reduction in fringe visibility. Non-uniform illumination is caused to some extent by misalignment, thus indicating a coupling effect. Also ruby crystals have been found to lase in thin filaments across the crystal face (Ref 14:23). Therefore the illumination is never uniform in intensity nor is it ever perfectly aligned for the duration of a long pulse, i.e., the time-averaged effect. Consequently, considering each filament as a source, illumination of the apertures is more uniform the smaller the aperture separation, although an oscillating filament may be located in any region of the crystal face. As a result, it is expected that the visibility would decrease with aperture separation, thus making it more difficult to isolate partial coherence effects from visibility measurements. This could also account for the significant

decrease in visibility from the predicted value for large aperture separations. Therefore the degree of spatial coherence found in this experiment is more of a lower limit of spatial coherence rather than the actual degree of coherence.

A better approximation to the actual degree of coherence could be obtained by compensating for the reduction in fringe visibility due to misalignment and non-uniform illumination. The amount of compensation required for non-uniform illumination could be determined by statistically measuring the ratio of complex amplitude magnitudes for each aperture separation and using Eqs (42) and (43) to arrive at the magnitude of the degree of spatial coherence.

The compensation required for misalignment could be determined in two steps. First a nearly perfect spatially coherent source (e.g. a continuous wave gas laser) could be used to determine the reduction in visibility for increasing angles of misalignment for each aperture separation. Then some measure of asymmetry could be chosen and plotted with visibility reduction as a function of aperture separation. Then using the adopted criterion of asymmetry, the ruby laser fringe pattern could yield a value of fringe visibility reduction through considerations of its degree of asymmetry and the particular aperture separation. This value of fringe reduction could then be used to increase the experimental values.

The use of both compensations in the magnitudes suggested above might yield a partial coherence effect greater than the actual case due to the coupling of the two factors. However, considerations of the particular experimental apparatus being used might present a

method of weighting the compensating factors to arrive at a good approximation of the partial coherence effect.

The final source of probable error lies in the theoretical prediction itself. The effects of aberrations were not included in the derivations. The effect of aberrations on partially coherent illumination is to introduce phase distortions within the band of frequencies passed by the optical system (Ref 8:121). This is important because the secondary source was assumed to be in the focal plane of the first microscope objective. Thus aberrations could change the spot size and geometry and could account for part of the apparent shift in the zeroes of the experimental curve from the predicted zeroes. Also, the paraxial approximations were used in the derivation of the transmittance function for a thin convex lens. But in the case of the first microscope objective and the lens L_2, the illumination exceeded the paraxial approximation by a great deal in the vertical direction thus causing the transmittance derivation to be questionable. However, these effects were minimized (if not negligible) by the fact that only the central portion of the incident beam was incident on the apertures and the axis of apertures was in the horizontal direction. So due to the small diameters of the apertures, the illumination that actually reached the film plane exhibited little effect of the excessive vertical extent of the illumination.

The high degree of correlation between the experimental and theoretical curves, based on an average of only three shots, suggests that the degree of coherence could be accurately determined by this experimental method if an average of twenty, or even ten shots, were

GSP/PH/70-12

used. Then with the aid of a computer the time averaged effective

radiation could be synthesized as explained earlier in this section.

This procedure could be performed at many levels of flash lamp excita-

tion (above threshold) resulting in a series of characteristic models

of the lasing radiation. The procedure could then be extended to a

statistical sample of lasers of similar specifications. The result,

in principle, would be a series of characteristic models of the time

averaged radiation that could be used by engineers in a manner similar

to the use of electron tube and transistor characteristic curves.

For this approach to be economically feasible, two requirements

must be met. First, a real time detector is needed. For example, a

light sensitive electronic package, that measured fringe visibility

directly and in real time, could eliminate two big time consumers—film

development and densitometer analysis. Next, an effective cooling

mechanism is needed to maintain the laser crystal temperature constant

at room temperature. This would leave detector response time as the

limiting factor for the length of the time intervals between pulses.

III. Measurement of Temporal Coherence

The temporal coherence properties of the time-averaged radiation field were determined with the aid of a Twyman-Green interferometer. Since the details of this experiment are quite similar to the spatial coherence experiment, this material is organized and presented in the sequence as before, i.e., description of equipment, experimental procedure, theory of operation, calculations, and discussion of results.

Description of Equipment

The equipment used to measure the temporal coherence was the laser source, a Twyman-Green interferometer, photographic film, a densitometer and X-Y plotter.

The Twyman-Green interferometer consisted of the collimating section of the diffractometer, a circular aperture, beam splitter, two optical flats, and an imaging section. The aperture was constructed by punching a 1.9 centimeter diameter hole into one of the screens used in the Young's experiment (0.159 centimeters thick and 5.08 centimeters square).

The beam splitter was a 5.08 centimeter diameter by 6 millimeter thick optical flat. It was mounted at an angle of forty-five degrees with the incident beam. The side of the beam splitter nearest the aperture was coated with a dielectric film with a reflectance of 0.554 at 0.6328 microns (measured with helium-neon gas laser), for incident illumination that is horizontally polarized, i.e., parallel to the plane of incidence.

Two, 2.54 centimeter diameter by 1.27 centimeter thick optical flats, were positioned in the path of the two beams leaving the beam
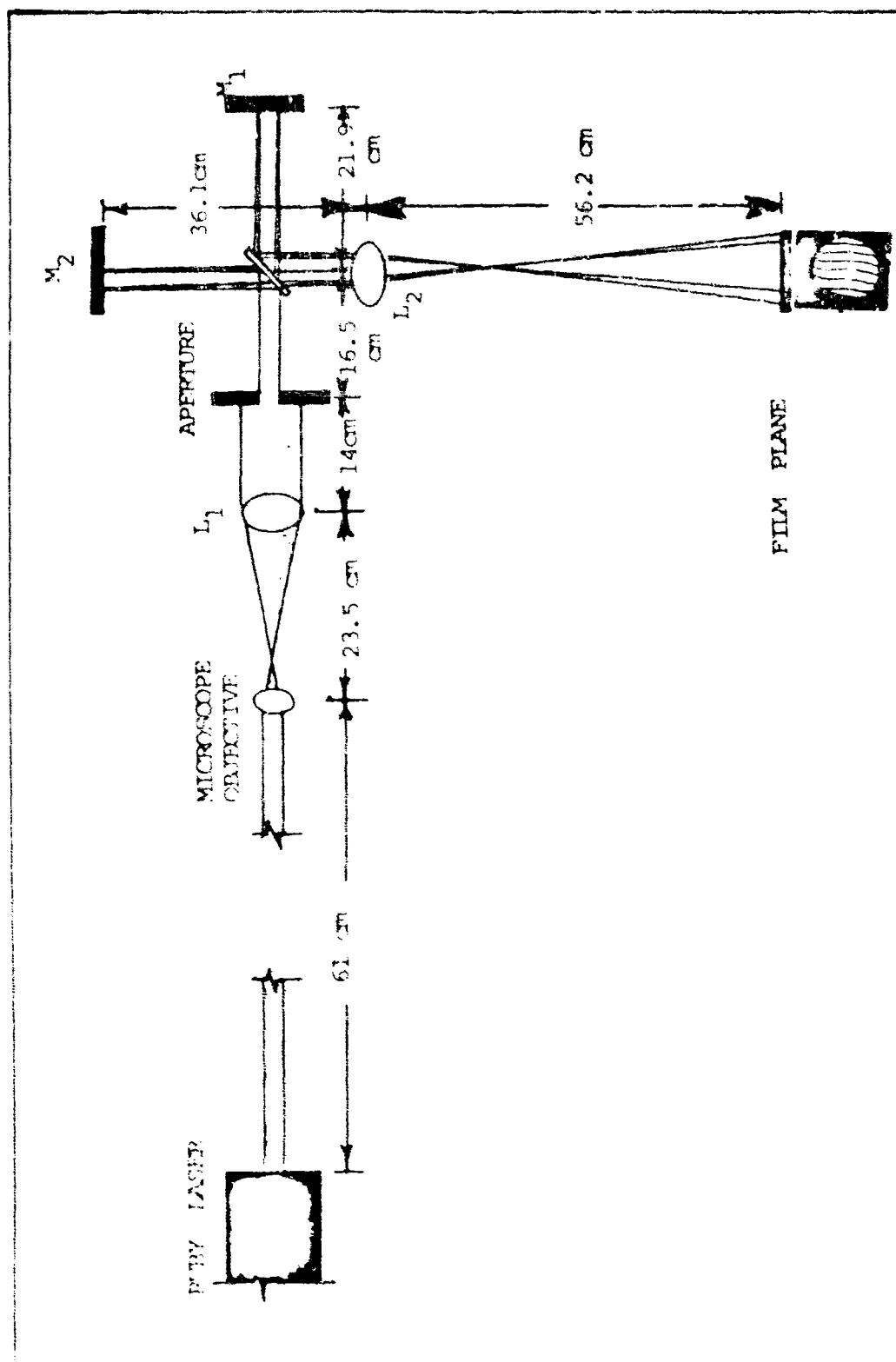
FIGURE 7a

TWYMAN – GREEN INTERFEROMETER

splitter. They were mounted such that one flat was positioned along
the axis containing the collimating section and aperture and the
other flat mounted on an axis perpendicular to this axis. The optical
flat holders permitted angular movement, in both the horizontal and
vertical planes, about a center pivot point. In addition, the flat
positioned along the collimating section-aperture axis, had the
capability of a small degree of translational movement in the vertical
direction and considerable translational movement along the colli-
mating section-aperture axis. The latter movement was controlled by
a micrometer movement in graduations of 1.27 millimeters. Also one
face, of each flat, was coated with a dielectric film with
a reflectance of 0.9, and the flats were oriented so that these
faces were the first to intercept the incident beams.

The imaging section contained a 4.25 diopter convex lens iden-
tical to the lenses, L_3 and L_2, used in the Young's experiment and
a film plate holder in the image plane, i.e., plane of desired
magnification. The film used was Kodak V-F Spectroscopic plate
(see Fig. 12).

The dimensions and orientations of the different elements of
the Twyman-Green interferometer are depicted in Fig. 7.

The densitometer and X-Y plotter were the same as used in the
Young's experiment.

Experimental Procedure

The laser-source was aligned with a helium-neon gas laser using
the same procedures described in the spatial coherence chapter.
Then the Twyman-Green interferometer was aligned. It was considered
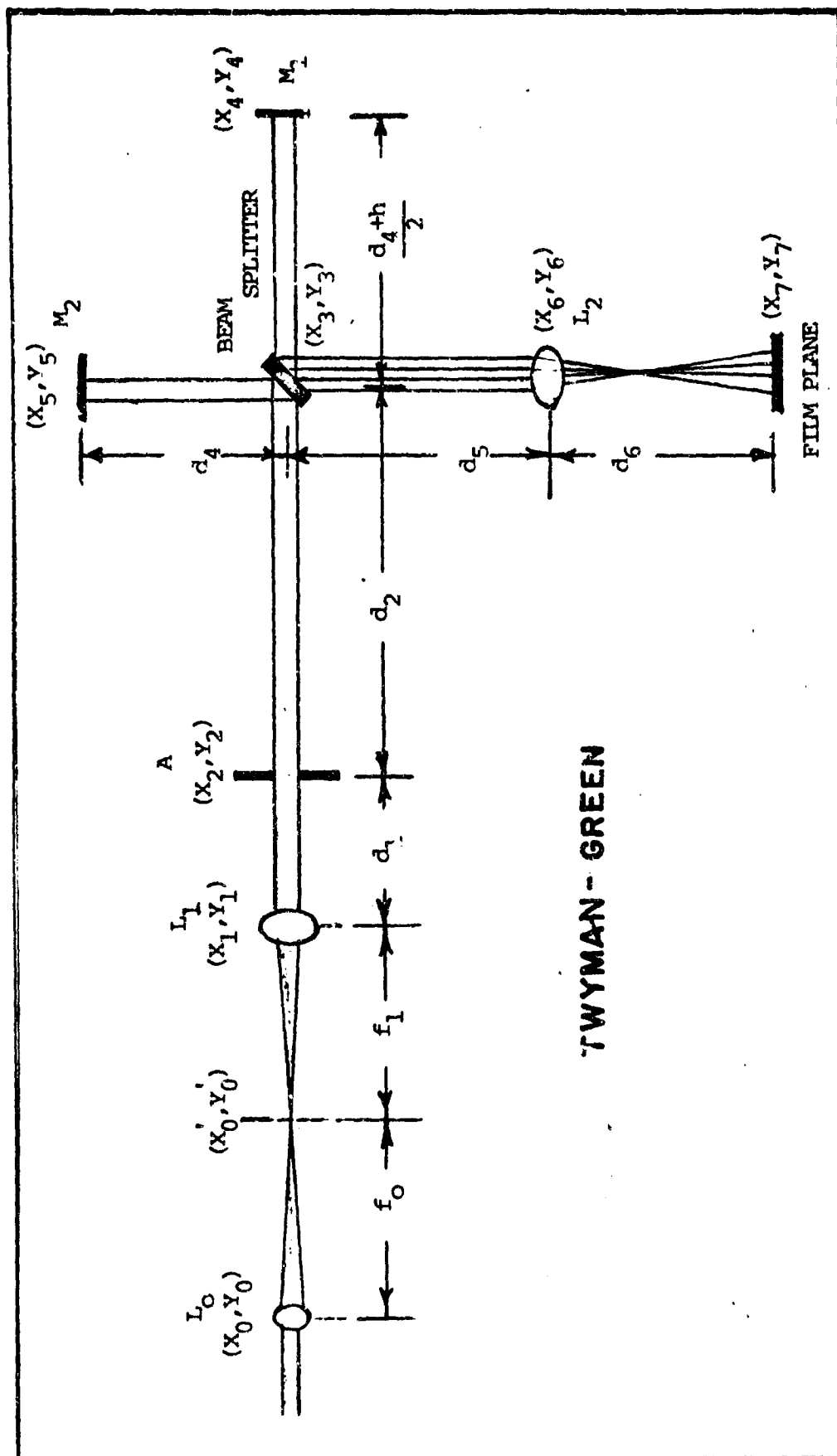
FIGURE 7b
THEORETICAL MODEL

aligned when a tilt of one mirror produced vertical fringes in the film plane. Finally, the source and the interferometer were aligned as a system.

After the system was properly aligned, the mirrors were positioned so that the paths traveled by the two beams were equal. The path lengths were measured with a steel tape. Consequently, these measurements were only a first approximation.

Next the laser was pulsed, the interference pattern recorded, and the movable mirror moved one micrometer graduation. This procedure was repeated with the result that interference patterns were recorded on both sides of the approximated zero path difference point.

The spectroscopic plates were developed and analyzed as described earlier.

Theory of Operation

The complex amplitude incident on the aperture A was identical to the illumination incident on the screen in Young's experiment, i.e.

$$U(x_2, y_2) \quad \left[\text{RECT} \left(\frac{x_2 f_o}{L_{x1}} \right) \quad \text{RECT} \left(\frac{y_2}{L_{r1}} \right) \right] \left(\frac{A f_o}{2 \pi f_1} \right) \qquad (44)$$

where the distance, d_1, from the lens L_1 to the aperture represented propagation deep within the Fresnel diffraction region.

The incident rectangular pulse was approximately 1.2 centimeters by 2.5 centimeters, whereas the diameter of A, was 1.9 centimeters. Thus the rectangular pulse was truncated in the vertical direction

and the illumination leaving the aperture was approximately elliptical in cross-sectional shape. Thus

$$U'(x_2,y_2) = \frac{Af_o}{2\pi f_1} \, CIRC \left(\frac{r_2'}{L_x L_A f_1} \right)$$

where

$$r_2' = \left[(f_o L_A x_2)^2 + (L_x f_1 y_2)^2 \right]^{1/2}$$

and

$$2L_A = \text{diameter of the aperture A}$$

The illumination proceeded to the beam-splitter through the Fresnel diffraction region. The beam-splitter was an optical flat of thickness d_o, thus light incident upon it experiences multiple reflections (see Fig. 8).

From the figure, it follows that the complex amplitude reaching M_1 was approximately

$$U(x_4,y_4) = att' \left[\sum_{n=0}^{\infty} (r'r''e^{J\delta_o})^n \right] e^{J\left(\frac{\delta_1+h}{2}\right)} K$$

$$= \frac{att'e^{J(\delta_1+h)\frac{K}{2}}}{1 - r'r''e^{J\delta_o}} \qquad \text{where } a = \frac{Af_o}{2\pi f_1} \tag{46}$$
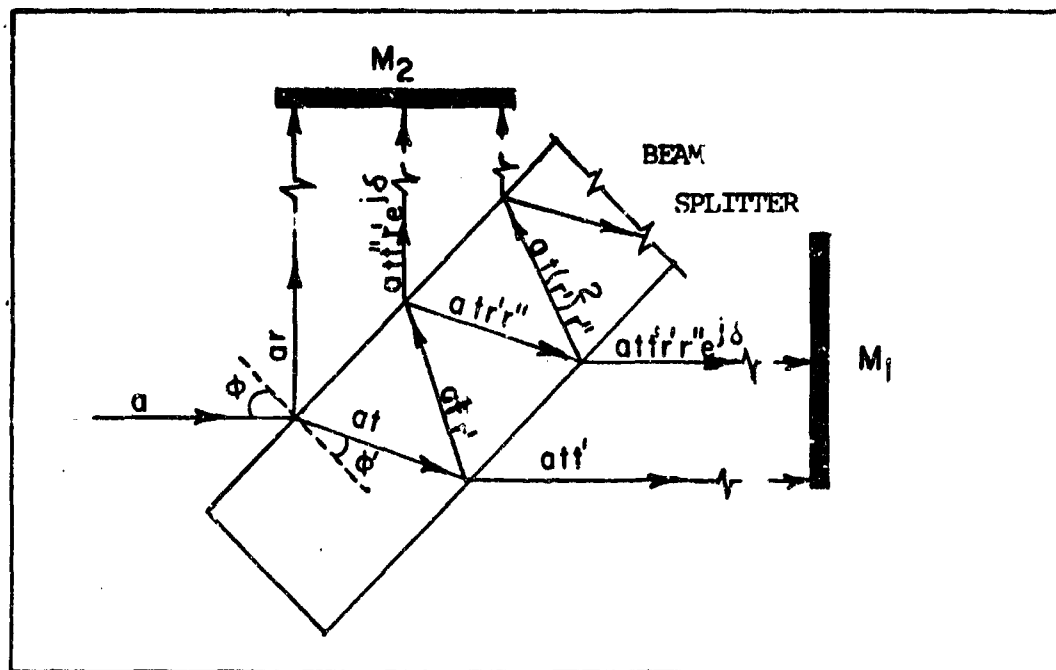
FIGURE 8

INCIDENT BEAM MULTIPLE REFLECTIONS

δ_o = Kn ($2d_o$ COS ϕ'), δ_1 = d_4, and r'' = $-r$, by Stokes Theorem.

The geometrical shape will be ignored until the complex amplitude is imaged by the lens L_2. Then

$$U'(x_4 y_4) = \frac{att'e^{J(\delta_1 + h)\frac{K}{2}}}{1 + r\,r'e^{J\delta_o}}$$

where r^2 is the reflectance of the dielectric coating and $(r')^2$ is the inside reflectance of the glass interface. The beam splitter has been assumed to be infinitely long since the amplitude of the re-flected beams decrease as powers of the reflectances.

The illumination was reflected and transmitted by the mirror M_1.

51

The reflected beam was incident upon the beam splitter where it was both reflected and transmitted again (see Fig. 9).
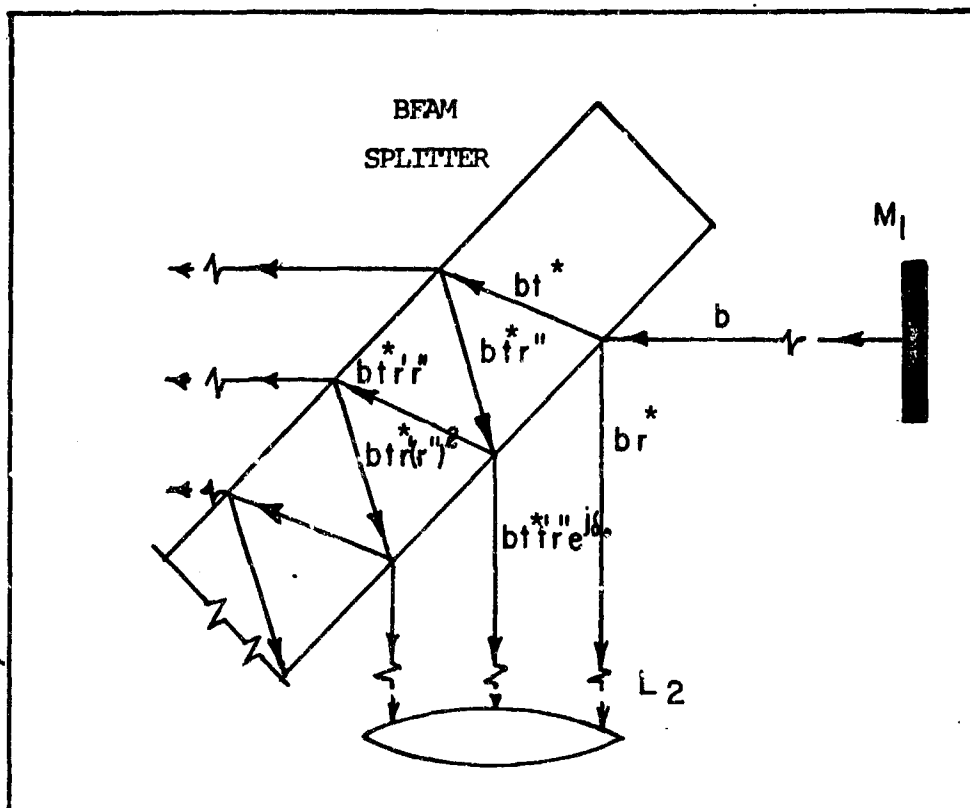
FIGURE 9

BEAM REFLECTED FROM M_1

Then the complex amplitude incident on the lens, L_2, is given approximately as follows:

$$U_{M1}(x_6,y_6) = br* + bt't*r''e^{J\delta_o}\sum_{n=0}^{\infty}(r''r'e^{J\delta_o})^n$$

$$= -\frac{att'e^{J(\delta_2+h)\frac{K}{1}}r_M}{1 + r r'e^{J\delta_o}}\left[r' + \frac{(1-r'^2)re^{J\delta_o}}{1 + r'}\right] \tag{47}$$

52

where $\delta_2 = d_4 + d$

The reflectance of the dielectric coating was measured at 0.6328 microns and found to be 0.55 ± 5% at a forty-five degree orientation and horizontal polarization. The polarization of the pulsed ruby laser was measured and the ruby crystal oriented such that horizontal polarization was achieved (see Appendix C). Thus the reflectance at 0.6943 microns is approximately 0.5, i.e.

$$r^2 \approx 0.5 \text{ or } r \approx 0.7$$

Considering Fresnel's laws of reflection and Snell's law, r' can be determined.

$$r' = \frac{TAN\ (\phi' - \phi)}{TAN\ (\phi' + \phi)} \approx \frac{TAN\ (-17^o)}{TAN\ (73^o)} = -0.093 \tag{48}$$

Then

$$U_{M1}(x_6, y_6) \approx -att'e^{JK(\delta_2 + h)}\ r_m\ \frac{(r' + re^{J\delta_o})}{(1 + r\ r'e^{J\delta_o})^2} \tag{49}$$

Similarly the complex amplitude incident on the mirror M_2 was as follows.

$$U_{M2}(x_5, y_5) \approx a\left[\frac{r + r'e^{J\delta_o}}{1 + r\ r'e^{J\delta_o}}\right] e^{J\delta_3}$$

And the complex amplitude incident on the lens, L_2, which had been reflected from the mirror M_2 was given by the following expression:

53

$$U_{M2}(x_6, y_6) \simeq \frac{att'(r + r'e^{J\delta_o}) \, r_m \, e^{J\delta_2}}{(1 + r \, r'e^{J\delta_o})^2} \tag{50}$$

where $\delta_2 = k'd_4 + d_5$.

The complex amplitude arriving in the film plane was

$$U(x_7, y_7) \simeq \frac{att'r_m d_5}{d_6(1 + r \, r'e^{J\delta_o})^2} \, CIRC\left(\frac{d_5 r_7'}{d_6 L_x L_A f_1}\right) \left[(r + re^{J\delta_o})\right.$$

$$\left. e^{JKh} + r + r'e^{J\delta_o}\right] \tag{51}$$

where only pertinent path differences are retained.

Then the intensity incident on the film for the average wave number ($\bar{\sigma} = 1/\bar{\lambda}$) was given by:

$$I(\bar{\sigma}) = I_{M1}(\bar{\sigma}) + I_{M2}(\bar{\sigma}) + 2[I_{M1}(\bar{\sigma})I_{M2}(\bar{\sigma})]^{1/2}$$

$$R_E\{\gamma_{11}(\bar{\sigma})e^{2\pi J\bar{\sigma}h}\} \tag{52}$$

where I_{Mi} = the intensity at the film plane due to the ith mirror, $\gamma_{11}(\bar{\sigma})$ = to the normalized degree of spatial coherence, and h = path difference of the two beams.

The degree of spatial coherence can be determined by Eqs (24), where the derivations from this point to the derivation of the total coherence function is essentially the method of Hopkins (Ref 10)

$$I(P) = \int_{\Sigma} \frac{I(\Sigma,\bar{\sigma})}{R^2} \, d\Sigma = \left(\frac{Af_o}{2\pi f_1 Z_o} \right)^2 \left[\frac{\pi L_x f_1 L_A}{f_o} \right]$$

$$\gamma_{11}(\bar{\sigma}) = [I(P)]^{-1} \int_{\Sigma} \frac{I(\Sigma,\bar{\sigma}) e^{J2\pi(R_1-R_2)\bar{\sigma}}}{R^2} \, d\Sigma$$

$$\gamma_{11}(\bar{\sigma}) = \frac{2J_1\left\{ \frac{2\pi L_x L_A f_1 \bar{\sigma}}{Z_o} \left[\left(\frac{h_1}{L_A f_o} \right)^2 + \left(\frac{h_2}{f_1 L_x} \right)^2 \right]^{1/2} \right\}}{\frac{2\pi L_x L_A f_1 \bar{\sigma}}{Z_o} \left[\left(\frac{h_1}{L_A f_o} \right)^2 + \left(\frac{h_2}{f_1 L_x} \right)^2 \right]^{1/2}} \tag{53}$$

Here h_1 and h_2 are the separations in the x and y-directions of the
film plane for a source point. Then $\gamma_{11}(\bar{\sigma})$, represents the spatial
correlation between the two separated images (due to the mirror tilt)
in the film plane. The illumination leaving the aperture (Eq (45))
was considered as the secondary source. Also Z_o, represents the
total distance from the aperture A, to the film plane.

To account for the finite frequency spread, the total intensity
was found by integrating $I(\bar{\sigma})$ over the spread of wave numbers.

$$I = I_{M1} + I_{M2} + 2(I_{M1}I_{M2})^{1/2} R_E\{J_{21}\}$$

where

$$I_{Mi} = \int_0^\infty I_{Mi}(\sigma) \, d\sigma$$

55

and

$$J_{21} = \int_0^{\infty} \left[\frac{I_{M1}(\sigma)I_{M2}(\sigma)}{I_{M1}I_{M2}} \right]^{1/2} |\gamma_{11}(\sigma)| e^{2\pi Jh\sigma} \, d\sigma \qquad (54)$$

Considering the values of r and r', then $I_{M1} = I_{M2}$. If the spectral distribution $\dfrac{I_{M1}(\sigma)}{I_{M1}}$ is considered, then the geometric mean energy distribution can be defined, i.e.

$$E(\sigma) = \left[\frac{I_{M1}(\sigma)}{I_{M1}} \frac{I_{M2}(\sigma)}{I_{M2}} \right]^{1/2} \propto \frac{1}{\Delta\sigma} \qquad (55)$$

Assuming the spatial coherence varies very little with wave number and that the profile of the spectral line is Gaussian, then the total coherence function (J_{21}) can be written as follows:

$$J_{21} = (e^{2\tau J\bar{\sigma}h}) \frac{2J_1(2\pi\xi)}{2\pi\xi} \; e^{-\pi(\delta\sigma h)^2} \qquad (56)$$

where $\delta\sigma \equiv$ to the width of the line profile at the points where the intensity has dropped to $e^{-\pi/4}$ of its value at the center of the line, and

$$\xi = \frac{L_x L_A f_1 \bar{\sigma}}{Z_o} \left[\left(\frac{h_1}{f_o L_A} \right)^2 + \left(\frac{h_2}{f_1 L_x} \right)^2 \right]^{1/2}$$

The temporal coherence can be defined as $W(h) = e^{-\pi(\delta\sigma h)^2}$. The Eq (54) for total intensity became

$$I = \left\{ \left(\frac{A f_o t t' r_m d_5}{2 \pi f_1 d_6} \right)^2 \Delta\sigma \; CIRC^2 \left(\frac{d_5 r_7'}{d_5 L_x L_A f_1} \right) \right.$$

$$\left. \left[1 + \frac{2 J_1 (2\pi\xi)}{2\pi\xi} \; e^{-\pi(\delta\sigma h)^2} \; COS \; (2\pi\bar{\sigma}h) \right] \right\} \tag{57}$$

and Eq (29) for visibility became

$$V = \frac{2 J_1 (2\pi\xi)}{2\pi\xi} \; e^{-\pi(\delta\sigma h)^2} \tag{58}$$

Consequently, if the visibility is plotted as a function of $h/2$, (movement of the mirror from the point of zero path difference), then the function graphed is approximately, $V = B \; e^{-\pi(\delta\sigma h)^2}$, i.e., Gaussian.

As discussed previously in the Young's experiment, the visibility (V') that is actually determined experimentally is an amplitude visibility function if photographic film is used as the detector and the intensity visibility function, V, is the square of V'.

The coherence time is given by (Ref 11:7-17)

$$(\Delta t)^2 \approx \frac{\displaystyle\int_o^\infty \tau^2 V^2(\tau) d\tau}{\displaystyle\int_o^\infty V^2(\tau) d\tau} = \frac{c^{-2} \displaystyle\int_o^\infty h^2 e^{-2\pi(\delta\sigma h)^2} dh}{\displaystyle\int_o^\infty e^{-2\pi(\delta\sigma h)^2} dh} \tag{59}$$

and

$$\Delta t = \frac{1}{2C\delta\sigma}$$

The coherence length is given by

$$\Delta L = C\Delta t = \frac{1}{2\delta\sigma} \quad \text{(Ref 3:319)}$$

Considering Eqs (49) and (50) it follows that

$$|U_{M1}| = |U_{M2}| = att'r_m \frac{(r^2 + r'^2 + 2r \ r'\cos\delta_o)^{1/2}}{1 + (r \ r')^2 + 2r \ r'\cos\delta_o}$$

and

$$V' = \left[\frac{2J_1(2\pi\xi)}{2\pi\xi} e^{-\pi(\delta\sigma h)^2} \right]^{1/2} \tag{60}$$

The mathematical model of the line shape has been assumed to be Gaussian. To complete this model, a value for $\delta\sigma$ must be assumed. The average value of Δh, at the $e^{-\pi/8}$ point from the maximum value of the amplitude visibility curve, was used in conjunction with Eq (59), to determine a value for $\delta\sigma$. Thus the theoretical prediction, assuming a Gaussian line shape, for the temporal coherence factor was

$$W(h) = e^{-\pi\left(\frac{N}{6.78}\right)^2}, \quad N = 0, 1, 2, \text{---} . \tag{61}$$

Examples of the recorded fringes are provided in Fig. 10.

Calculation

    The film and densitometer traces were prepared using identical procedures to those used in the spatial coherence experiment.

    The densities were calculated using the same relations as before. The slopes of the Hurter-Driffield curves (gammas) were determined for each density point instead of the secant line approximation technique used in the previous experiment.

    Having determined the gammas, the amplitude visibility was determined by

$$\gamma' = \frac{(t_{min})^{-\frac{1}{\gamma_{min}}} - (t_{max})^{-\frac{1}{\gamma_{max}}}}{(t_{min})^{-\frac{1}{\gamma_{min}}} + (t_{max})^{-\frac{1}{\gamma_{max}}}} \qquad (62)$$

Here t is amplitude transmittance as determined by the densitometer trace within a constant factor as explained in the previous experiment. Then V' was squared to arrive at the intensity visibility function (V). The intensity visibility was then plotted as a function of micrometer movements as depicted in table II and graph II.

Discussion of Results

    To achieve the maximum correlation between the spatial and temporal coherence experiments, the experimental apparatus was changed as little as possible. The laser source was not altered and comments on mode selection and mode control presented in the discussion of the first experiment still apply. However in this experiment, the

(0.5mm x 3microns slit size & 0.5 mm/min scan speed)

(b) 2.54mm Path Difference
0.1 Neutral Density Filter

(a) 0- Path Difference

(c) 7.62mm Path Difference
0.2 Neutral Density Filter

(e) -7.62mm Path Difference
0.3 Neutral Density Filter

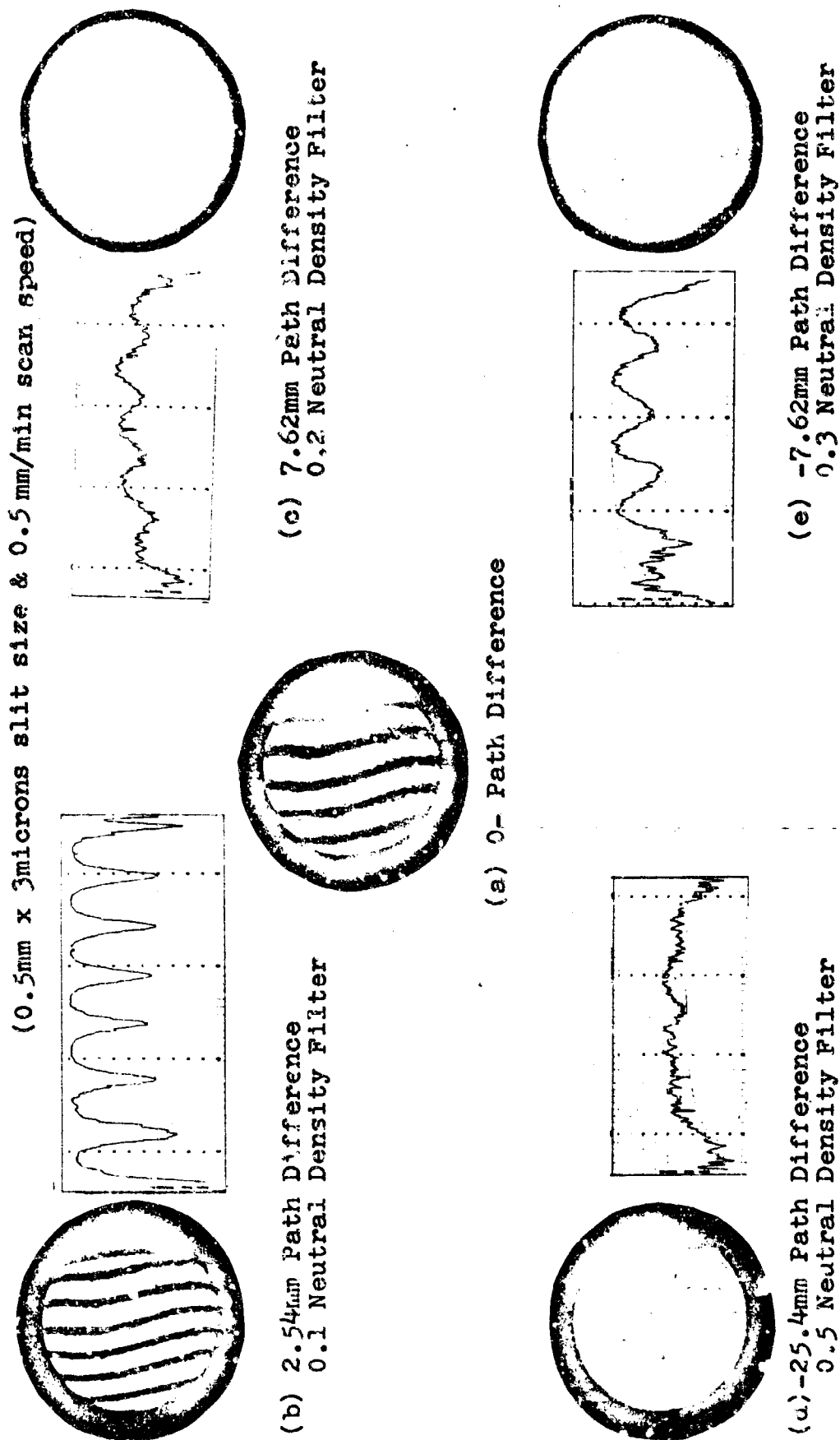(d) -25.4mm Path Difference
0.5 Neutral Density Filter

FIGURE 10

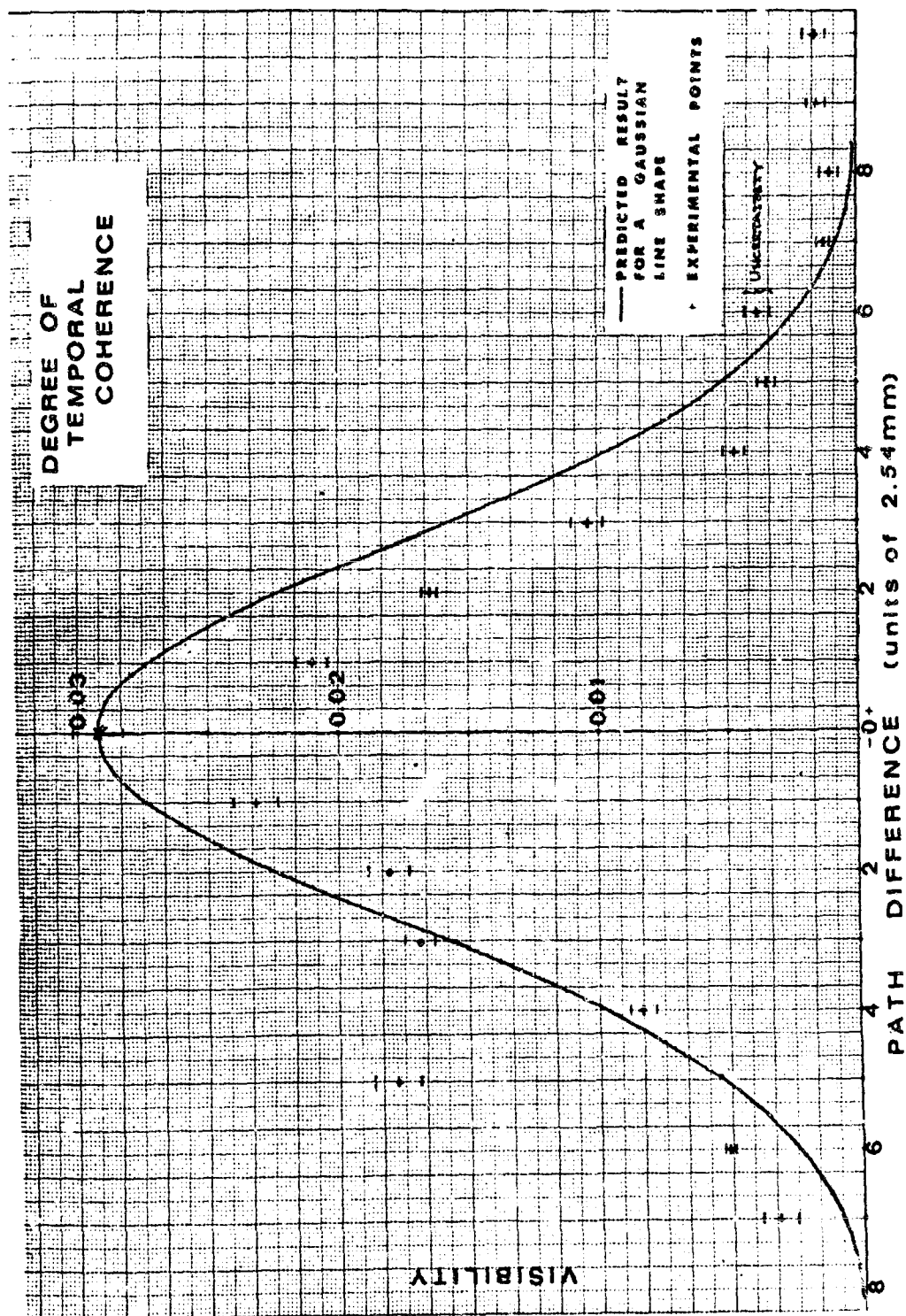TYPICAL INTERFERENCE FRINGES & DENSITOMETER TRACES FOR TEMPORAL COHERENCE

FIGURE 11

GRAPH II - DEGREE OF TEMPORAL COHERENCE

multiple transverse modes were essentially independ?nt of the temporal coherence measurements. The statistical nature of the radiation was unchanged since the laser source was not altered. Due to the quantities being measured, the statistical variaticn was now evident in the emission of longitudinal modes.

Three shots were again the sample size. This fact, in conjunction other sources of possible error caused a significant degree of uncertainty to accompany some experimental results. A discussion of these possible sources of error and an estimate of the maximum degree of uncertainty connected with each will be discussed next.

The manufacturer did not provide a graph relating gamma and development time for the V-F Spectroscopic plates. Therefore the H-D curve was the only source from which values for gamma could be obtained. The uncertainty in the determination of gamma was negligible in comparison with the first experiment for two reasons. First, the gamma values were determined for each point separately instead of computing an average gamma for each pair of points by using the secant approximation. Also the H-D curves had very little curvature except for plates of low density ($D \leq 0.5$).

The variation in visibility due to an uncertainty in the determination of the amplitude transmittance will be considered next. This uncertainty was due to three sources of possible error--the accuracy of the densitometer-recorder combination, non-uniform density of the unexposed film, and the accuracy to which the signal could be differentiated from the noise on the graphs prepared by the X-Y recorder. The non-uniformity of film density was neglected, but

it does represent a potential systematic error. However, since the non-uniformity is a random phenomena, the error should be negligible since a large number of plates (60 plates) constituted the experimental data source. The problem of differentiating signal from a noise background was negligible in the spatial coherence experiment. However, for the temporal coherence measurements, the noise was of such magnitude, that the signal was almost obscured at large path differences. This noise was caused, to a large extent, by parallel-plate fringes due to the beam splitter and to a lesser extent, by dust and aberrations.

The procedures used to estimate the maximum error in intensity visibility due to an uncertainty in amplitude transmittance parallel those used in the spatial coherence experiment. The inherent accuracy of the densitometer-recorder combination was estimated as one per cent of the full scale deflection. The maximum error due to noise was estimated by averaging the maximum uncertainty due to noise in the transmittance for each micrometer setting (path difference). Then the maximum error in amplitude visibility as a function of transmittance uncertainty was computed using Eqs (38) and (62), i.e.

$$\Delta V_t^{'} = \frac{2 t_1^{-\frac{1}{\gamma_1}} t_2^{-\frac{1}{\gamma_2}}}{\left(t_1^{-\frac{1}{\gamma_1}} + t_2^{-\frac{1}{\gamma_2}} \right)^2} \left(\frac{\Delta t_D + \Delta t_{1N}}{\gamma_1 t_1} + \frac{\Delta t_D + \Delta t_{2N}}{\gamma_2 t_2} \right) \qquad (63)$$

Here Δt_D, is the uncertainty due to the densitometer recorder combination and Δt_1 is the uncertainty due to noise. The imprecision in

63

KODAK Spectroscopic Plate and Film, Type V-O Tungsten exposure; D-19 Developer

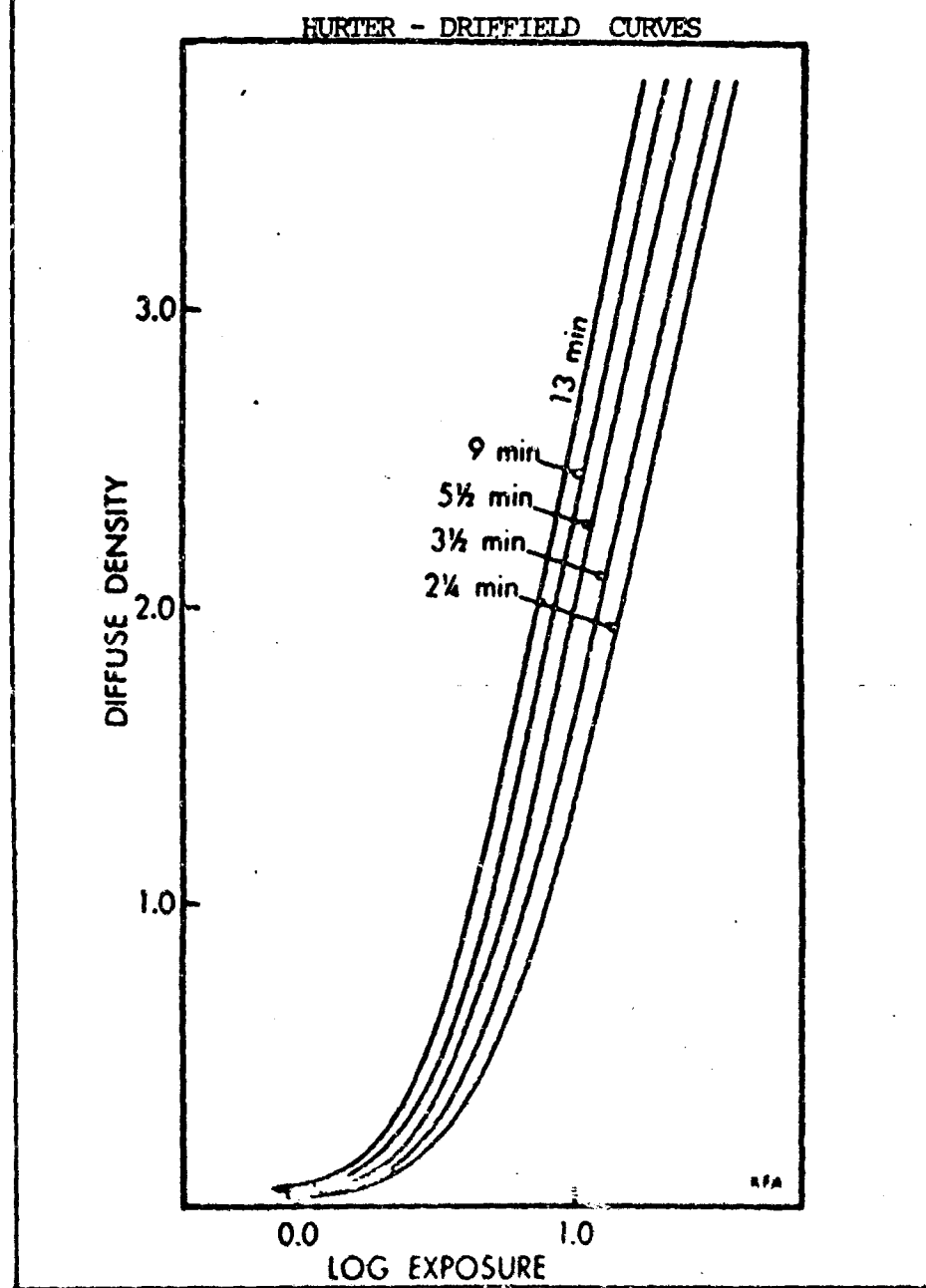HURTER - DRIFFIELD CURVES

FIGURE 12

HURTER - DRIFFIELD CURVES FOR V-F SPECTROSCOPIC PLATES

amplitude visibility due to the statistical nature of the radiation was estimated next. The maximum deviation of an experimental point from the arithmetic average was used to estimate this imprecision.

The maximum errors in the amplitude visibility that were computed above were combined and used in conjunction with Eq (40), to arrive at an estimate of the maximum error in the intensity visibility function. The results of these calculations are depicted in graph II.

The sources of possible error, the magnitudes of which could not be estimated, were of the same nature as those present in the first experiment, i.e., crystal temperature at the time of lasing action not constant, possibility of varying levels of flash lamp excitation, misalignment of the source and the optical axis of the interferometer, filament oscillation within the ruby crystal, and unequal magnitudes of the complex amplitudes arriving at the film plane. The latter three sources of error have the same type of effect on the temporal coherence measurements. They cause the magnitudes of the complex amplitudes (from the two mirrors) to be unequal and also decrease the spatial coherence. These two factors then decrease the visibility. However, this decrease should be quite small when compared with that caused by the presence of multiple longitudinal modes. In fact, the visibility measured was less than the predicted single mode behavior by a factor of thirty-four. This reduction in visibility will now be considered in more detail.

The Twyman-Green interferometer provides a field of view which is uniformly illuminated at the zero path difference and zero angle

of inclination conditions of the two mirrors. Angle of inclination implies a change from the perpendicular orientation of the mirrors. In this experiment, the mirrors were purposely tilted to obtain straight line fringes so that their contrast could be measured. This tilt caused the super imposed images to separate. Misalignment of the source and the axis of the interferometer and also filament oscillation would tend to increase this separation. The degree of spatial coherence is a measure of the correlation between the images which are being separated. Consequently, the amount of tilt and the misalignment of the source (including the time averaged effect of the filament oscillations) decrease the spatial coherence by increasing the image separation. Misalignment was interpreted as the deviation of the direction of propagation of the incident illumination from the optical axis of the interferometer.

If the amount of tilt of the mirrors was held constant for each shot, then the reduction in spatial coherence due to this factor would be constant. The experimental visibility could be multiplied by an appropriate constant and this error essentially removed. However, a review of the fringe patterns reveal that the number of fringes, and thus the amount of tilt, was not constant for each shot. But the variation in the number was small (see Fig. 10). Considering Eq (56), and the actual values of the various parameters, it can be shown that $\xi \approx 10^2 [(h_1/15)^2 + (h_2/145)^2]^{1/2}$ millimeters. Thus for the small separations considered in this experiment (separations of the order of a small fraction of a millimeter), the spatial coherence changes very little   fact, separations as much as one-tenth of a

millimeter would reduce the spatial coherence to only 20% of its zero separation value. Thus the reduction in visibility due to reduced spatial coherence could not be responsible for the large decrease from the predicted values.

The next factor capable of reducing the visibility is unequal magnitudes of the complex amplitudes. These magnitudes were shown to be equal based on approximations concerned with the values determined for the reflectances of the dielectric coating (r^2) and the opposite glass face $(r')^2$ of the beam splitter. These values of reflectance were based on the assumption that the beam splitter was positioned at an angle of forty-five degrees with the incident beam. However, this positioning was done by visually judging this angle. Thus this setting could not be more accurate than a few degrees. This positioning technique was also used in the measurement of the reflectance of the dielectric coating at the forty-five degree inclination. Thus the positioning error could possibly have doubled in the process of determining the reflectance at a particular inclination and then placing the beam splitter in the experimental apparatus at this inclination.

The reflectance is a function of wave length through the index of refraction (N). Considering the Cauchy equation for normal dispersion

$$N = A + \frac{B}{\lambda^2} + \frac{C}{\lambda^4} \quad \text{(Ref 12:468)}$$

it is obvious that an increase in wavelength implies a decrease in

index of refraction. Using Fresnel's law of reflection for parallel polarization (Eq (48)), it can be shown that

$$r^2 = \left(\frac{N \cos \phi - \cos \phi'}{N \cos \phi + \cos \phi'}\right)^2 \tag{64}$$

This equation, when the values of ϕ and ϕ' are considered, illustrates that a decrease in index will cause a corresponding decrease in the reflectance. Also, if the rate of change of the reflectance with index is inspected, we find that the rate of change of reflectance increases with a decrease in index. The rate of change is given by

$$\frac{\partial(r^2)}{\partial N} = \frac{4 \cos \phi \cos \phi' (N \cos \phi - \cos \phi')}{(N \cos \phi + \cos \phi')^3} \tag{65}$$

The relevance of this analysis lies in the fact that the value of the reflectance was determined at 6328 A^o (helium-neon continuous wave gas laser), but the beam splitter was utilized at 6943 A^o. Therefore this small increase in wavelength, coupled with the inaccuracy in the forty-five degree inclination positioning creates the possibility of an amplitude mismatch in the film plane.

During the process of measuring the reflectance, the beam splitter was found to exhibit marked preference for polarizing angle. The two equal beams were provided when the polarization was parallel to the plane of incidence. However, the polarization experiment with the pulsed laser (appendix C) showed only a preferred plane of polarization. This could only cause a further increase in the

68

amplitude mismatch and corresponding decrease in visibility.

The possibilities of unequal amplitudes appear to be quite plausible. However, the magnitude of the decrease in visibility that it might have caused does not appear to be significant. As pointed out in the earlier discussion of Eq (43), the amplitude mismatch must be quite large to cause a significant decrease in visibility.

Only the presence of multiple longitudinal modes remains as the possible reason for the significant decrease in the visibility. Equation (32), describes the manner in which multiple modes combine to decrease the visibility. Since still photography was used as the detection mechanism, only the time-averaged effect of the multiple modes could be observed. Consequently, the theoretical curve was normalized downward to the same order of magnitude as the experimental points to determine the amount of deviation from the single mode predicted curve shape. The experimental points indicated that the actual visibility decayed faster than the predicted curve for path differences up to ± two centimeters. At this point, the signal to noise ratio of the graphs of relative transmittance became sufficiently large to cause the reliability of the data to be in question.

The experimental points appeared to be shifted from the center axis of the symmetric predicted curve. This situation has two probable causes. First, the zero path difference point was determined by changing the path difference on both sides of the calculated zero difference point and then analyzing the resulting fringe patterns. The position of the mirror that corresponded to the fringe pattern exhibiting the maximum contrast was chosen as the zero path difference

point. The smallest micrometer movement on the experimental apparatus was 1.27 millimeters. Consequently, this was the maximum accuracy to which the zero path difference could be measured with reasonable precision.

The next probable cause of the apparent shift in the experimental curve was its asymmetry. This asymmetry could be the result of a small misalignment caused by the time-averaged effect of filamentary oscillation. Also a blue shift in emission frequency, due to a uniform decrease in optical cavity length, which in turn is postulated to be directly proportional to changes in population inversion, has been detected by Wolga and Flamholz (Ref 22:2723). This phenomena was present in both Q-Switched and pulsed ruby lasers, regardless of laser power.

The anomaly at minus five units has a number of probable causes. It could be the result of secondary reflection. The statistical sample could be too small to localize the visibility at this path difference. However, the probability of this being the predominant cause is quite low due to the precision of the measurements obtained for this value of path difference and the proximity of the other seventeen experimental points to the predicted curve. The most probable cause of this anomaly is the time-averaged addition of multiple modes at this point.

The experimental results appear to indicate that the time-averaged output does approximate the effect of a single longitudinal mode for an input of 781.3 joules. A better approximation of the time-averaged radiation could be obtained with the aid of the computer as explained in the discussion of the spatial coherence experiment.

Now that the time-averaged coherence properties of the laser have been analyzed, the next step is to improve these characteristics. The present analysis could be used to evaluate any potential improvement mechanism or procedure.

The suggested approach toward improvement is to first, place an aperture in the laser cavity to improve the spatial coherence. Then the temporal coherence could be improved by placing a sapphire etalon or a dye cell in the cavity.

An attempt to improve the spatial coherence using a one millimeter aperture indicated that the exact location of the aperture in a plane perpendicular to the cavity is quite critical. In fact, an arbitrary placement of the aperture in a plane near the output mirror reduced the temporal and spatial coherence obtained in the non-mode selected case. This was probably the result of having blocked the dominant transverse mode, which was also the dominant longitudinal mode, by the aperture. Thus the aperture problem reduced to one of locating the area within the cavity where the probability of finding the dominant mode is highest. This could be determined in several ways. One method would be to photograph the face of the ruby crystal during lasing action. This should be done with a shutter speed comparable to the pulse duration so that the time averaged lasing is observed. Then, with the aid of neutral density filters, the location and size of the aperture can be determined. The size and location of the aperture can be approximately determined by examining the crystal in the Twyman-Green interferometer. Then those parts of the crystal face exhibiting scattering centers or other crystal defects would be

blocked by the aperture. In either case the dominant modes would be passed and competing modes would be blocked. Further experimentation might indicate a preference for the aperture along the length of the cavity.

Once the optimum aperture is installed in the optimum location, then the time-averaged spectrum should be observed. Using the fact that the longitudinal modes are spaced at regular intervals, the etalon can be placed in a location such that only the dominant longitudinal mode has high gain. Then the particular orientation of the etalon that produces the maximum degree of temporal coherence can be determined by experimentation. This procedure could be extended to two or more etalons, thus increasing the boundary conditions that an oscillation must satisfy, until the desired degree of coherence is obtained. However, this tailoring of the coherence properties is only valid at this one level of flash lamp excitation. Increased power requirements may necessitate redesign of the aperture and the relocation of the etalons. In fact, it is reasonable to expect that the dominance of any one mode would decrease as the excitation was increased much above twenty percent over the threshold excitation.

IV. Summary and Conclusions

The purpose of this study was to evaluate the coherence properties of a pulsed ruby laser for holographic applications.

The internal processes occurring within the laser cavity were not treated, but some processes were mentioned briefly in relation to some considerations of the radiated field. The time-averaged effect of the radiation field, as detected by photographic emulsion, was used as the basis for the discussion of the coherence properties. However, some aspects of the instantaneous radiation field were considered in interpreting the experimental results.

The laser was operated at room temperature and approximately twenty percent above threshold. Also, no mode selection was employed and the emitted radiation field was a statistical phenomenon.

The coherence properties were considered in terms of the spatial and temporal coherence properties. These two types of coherence were isolated by judicious choices of experimental arrangements. A form of Young's experiment was selected to isolate the spatial coherence effects and a Twyman-Green interferometer was used to study the temporal coherence properties. With the aid of these experiments, the time-averaged effect of the radiation field was detected and compared with a single mode theoretical prediction. This prediction was based on a scalar wave analysis and paraxial approximations. In addition, in the case of the temporal coherence prediction, the profile of the spectral line was assumed to be gaussian.

The results of the experiments were, for a 0.51 millimeter radius sample of a 2.54 centimeter diameter beam, a spatial

coherence length of approximately 2.2 millimeters, and, for the same beam size, a temporal coherence length of 1.27 centimeters. Consequently, the laser could be used as a holographic source for holograms requiring coherence lengths less than the above figures. However, for most holographic work these coherence properties were unsatisfactory--especially the temporal coherence properties.

The uncertainty of the experimental results were due to three main sources. They were the statistical nature of the radiation field, multimoding, misalignment of the source and the experimental apparatus, and variable laser parameters (crystal temperature, excitation voltage, etc.). These sources of uncertainty are listed in the order of decreasing effect on the experimental data.

Considering the objective of this study--analysis is incomplete in two respects. First, only one sample size (aperture size) was used in the spatial coherence experiment. This experiment should be repeated with different aperture sizes. Second, both experiments were performed with one level of excitation. The several spatial coherence experiments and the temporal coherence experiment should be performed at levels of excitation spanning the range from threshold to the maximum manufacturer suggested excitation. The subsequent analysis of these results would represent a complete study of the laser coherence properties.

In addition to the determination of the coherence properties of the source for an aperture size and an excitation level, this study accomplished two things. First, it shows that the approach used is feasible. However, a real time detector and a cooling process that maintains the crystal temperature constant is needed to make this

74

approach practical. The second accomplishment is the fact that
the quantitative results of this study can serve as a reference
point for improving the coherence of the laser by employing mode
selection.

Bibliography

1. Beran, Mark J. and George B. Parrent, Jr. Theory of Partial Coherence. Englewood Cliffs, N. J.: Prentice-Hall, Inc., 1964.

2. Boardman, Lt John D. "A Method for Analyzing Pulsed Laser Polarization." Proceedings of the Third Quarterly DOD Conference (1964) On High Power Laser Technology, AFAL-TR-65-93. Wright-Patterson Air Force Base, Ohio: Air Force Avionics Laboratory Research and Technology Division, August 1965.

3. Born, M. and Emil Wolf. Principles of Optics (Second Edition). New York: The MacMillan Company, 1964.

4. Chang, W. S. C. and J. W. Gray. A Discussion of Partial Coherence as Related to Optical Masers. AF33(657)-10824. Columbus, Ohio: The Ohio State University Research Foundation, May 1963.

5. Chang, W. S. C. and Neil R. Kilcoyne. "A Study of Partial Coherence and Its Application to the Collimation of Pulsed Multi-Mode Laser Radiation." Applied Optics, 4: 1404-1411 (November 1965).

6. Damon, Edward K. Focusing Optics For Intense Laser Sources. AF33(657)-10824. Columbus, Ohio: The Ohio State University Research Foundation, December 1963.

7. Evtuhov, V. and J. K. Neeland. "Pulsed Ruby Lasers." Lasers, Edited by Albert K. Levine. New York: Marcel Dekker, Inc., 1966.

8. Goodman, J. W. Introduction to Fourier Optics. St. Louis: McGraw Hill Book Company, 1968.

9. Gradshteyn, I. S. and I. M. Ryzhik. Tables of Integrals, Series and Products, Translated From Russian by Alan Jeffrey. New York: Academic Press, 1965.

10. Hopkins, H. H. "The Theory of Coherence and its Applications." Advanced Optical Techniques, Edited by A. C. S. Van Heel. New York: John Wiley and Sons Inc., 1967.

11. Heard, H. G. Laser Parameters Handbook, Vol. III. RADC-TR-66-704. Griffiss Air Force Base, New York: hnu Systems, Inc., Processed for Defense Documentation Center and Defense Supply Agency, February 1967.

12. Jenkins, Francis A. and Harvey E. White. Fundamentals of Optics (Third Edition). New York: McGraw Hill Book Company, 1957.

13. Jackson, John D. Classical Electrodynamics. New York: John Wiley and Sons, Inc., 1967.

14. Kilcoyne, Neil R. A Study of the Focusing and Collimating Properties of the Pulsed Multi-Moding Ruby Laser. AF33(657)-10824. Columbus, Ohio: The Ohio State University Research Foundation, December 1964.

15. Meadors, John G. Studies in Partial Coherence and Nonlinear Optics. AF33(657)-10824. Columbus, Ohio: The Ohio State University Research Foundation, November 1964.

16. Meadors, John G. and S. Bell. On Coherence Properties of a Light Beam as Measured in a Double Slit Diffraction Experiment. AF33(657)-10824. Columbus, Ohio: The Ohio State University Research Foundation, December 1964.

17. Smith, Howard M. Principles of Holography. New York: Wiley-Interscience, 1969.

18. Smith, William V. and Peter P. Sorokin. The Laser. New York: McGraw Hill Book Company, 1966.

19. Stroke, George W. and Robert C. Restrick III. "Holography With Spatially Non-Coherent Light." Applied Physics Letters, 7: 229-230 (November 1965).

20. Thompson, Brian J. Some Comments On The Measurement of $g_{12} = |\gamma_{12}(0)|$. Burlington Mass.: Technical Operations Research, 1964.

21. Thompson, Brian J. and Emil Wolf. "Two Beam Interference With Partially Coherent Light." Journal of the Optical Society of America, 47: 895-902 (October 1957).

22. Wolga, G. J. and A. Flamholz. "Transient Interference Studies of Passively Q-Switched Ruby Laser Emission." Journal of Applied Physics, 39:2723 (1968).

Appendix A

Table I

Visibility Calculations for Spatial

Coherence Experiments

Aperture Separation		Gamma Calculated	Visibility	(Visibility)^2
1	mm	0.731	0.989	0.978
2	mm	1.052	0.447	0.199
2.5	mm	1.005	0.314	0.098
3	mm	1.02	0.56	0.313
4	mm	1.068	0.331	0.109
4.5	mm	1.051	0.338	0.114
5	mm	1.01	0.296	0.087
5.5	mm	1.101	0.316	0.099
6	mm	1.017	0.14	0.019
6.5	mm	0.996	0.232	0.053
7	mm	1.018	0.335	0.112
8	mm	0.931	0.214	0.045
8.5	mm	0.8	0.056	0.003
9	mm	1.12	0.128	0.016

		Gamma (Linear Portion)		
1	mm	1.12	0.935	0.874
2	mm	1.12	0.422	0.178
2.5	mm	1.12	0.291	0.084
3	mm	1.12	0.559	0.312
4	mm	1.12	0.316	0.099
4.5	mm	1.12	0.319	0.101
5	mm	1.12	0.268	0.071
5.5	mm	1.12	0.311	0.096
6	mm	1.12	0.128	0.016
6.5	mm	1.12	0.207	0.042
7	mm	1.12	0.306	0.093
8	mm	1.12	0.179	0.032
8.5	mm	1.12	0.043	0.001
9	mm	1.12	0.128	0.016

Appendix B

Table II

Visibility Calculations for Temporal

Coherence Experiment

Path * Difference	Amplitude Visibility	Intensity Visibility	Uncertainty (ΔV)
-7	0.0561	0.0031	0.01268
-6	0.0511	0.0026	0.00335
-5	0.1292	0.0166	0.01672
-4	0.0808	0.0065	0.01025
-3	0.1185	0.0140	0.01154
-2	0.1348	0.0181	0.0159
-1	0.1563	0.0244	0.0167
0	0.1713	0.0293	0.01923
1	0.1457	0.0215	0.0123
2	0.1258	0.0158	0.00574
3	0.1053	0.0110	0.01231
4	0.0715	0.0051	0.00881
5	0.0574	0.0032	0.00642
6	0.0545	0.0029	0.00842
7	0.0374	0.0033	0.0044
8	0.0434	0.0018	0.00668
9	0.0341	0.0011	0.00707
10	0.0553	0.0030	0.00905
11	0.0323	0.0010	0.00105

* Units of 2.54 Millimeters

79

Appendix C

Preferred Plane of Polarization

The radiation from pulsed ruby lasers is generally partially plane polarized. Due to the short duration and high power of the laser output, the normal means of measuring the polarization (polarizer-analyzer combinations) can not be used.

A Brester-angle cone was used as an inexpensive way to measure the preferred plane of polarization. Then the crystal was rotated until the desired plane of polarization was achieved. The equipment and the experimental procedure are discussed below.

Description of Equipment

The equipment consisted of a laser source, a collimating section, circular aperture, a Brewster-angle cone, and spectroscopic film plates. The laser source and collimating section were identical to the ones used in the spatial and temporal coherence experiments. The circular aperture was a 0.32 centimeter diameter hole punched into a 5.08 centimeter square and 0.159 centimeter thick aluminum sheet. The Brewster-angle cone was constructed of crown glass with an index of refraction of 1.54 at 0.6943 microns and a Brewster's angle of 56 degrees and 33 minutes (Ref 2:94). The base of the cone was 2.5 centimeters in diameter and the height of the cone along its axis of revolution was two centimeters. The base of the cone was coated with an opaque film and then glued to a rectangular glass plate. The glass plate was 16.35 x 11 centimeters in area and 0.25 centimeters thick.
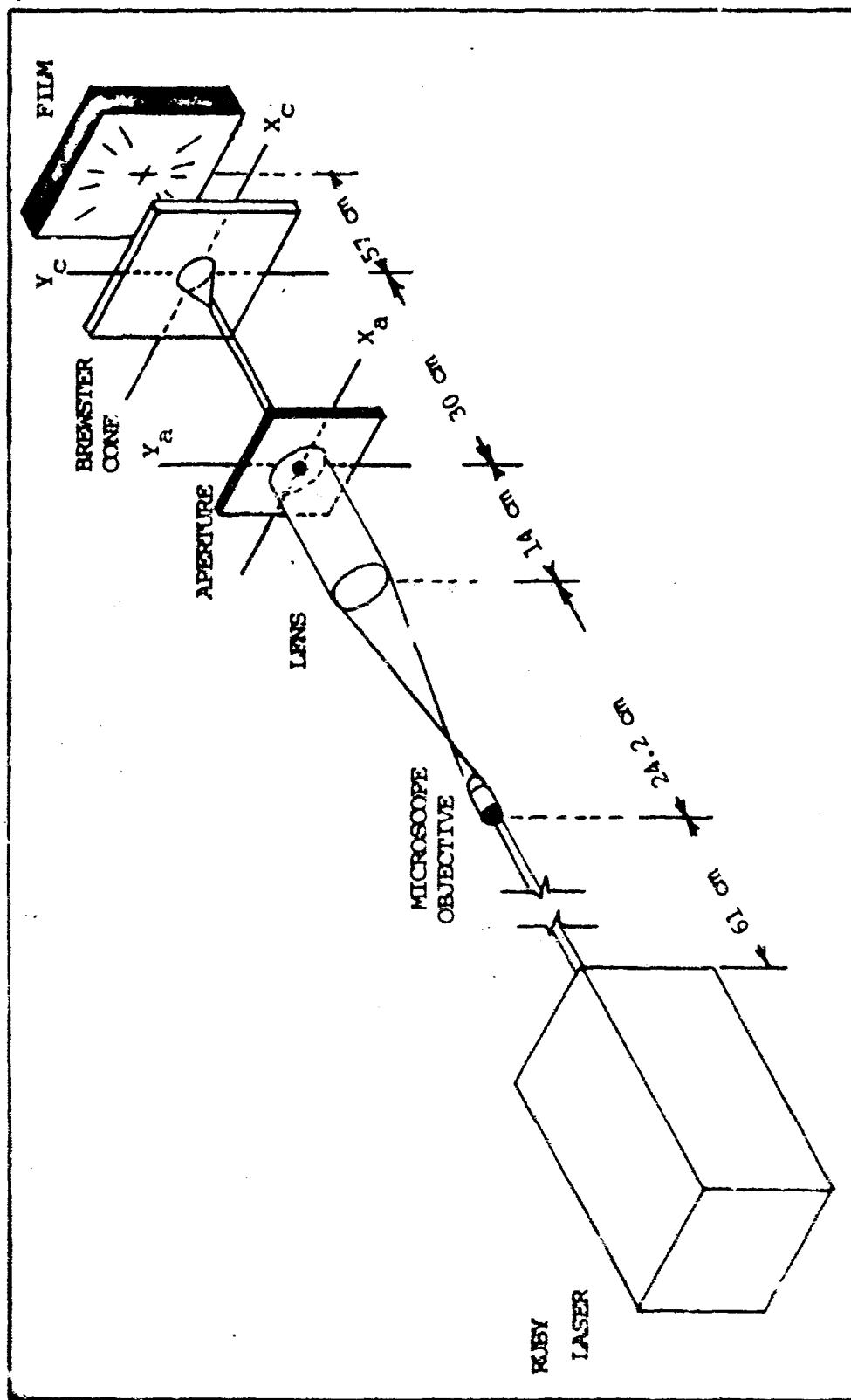
FIGURE 13

POLARIZATION EXPERIMENT

The film was Kodak 103-F Spectroscopic plates which were mounted in a holder 5.72 centimeters behind the glass plate. The dimensions and orientations of the elements are depicted in Fig. 13.

Theory of Operation

The collimating section converted a plane-polarized wave into a plane-polarized wave of larger cross-section. Thus the complex amplitude incident on the circular aperture was $U(x_a, y_a)$.

$$U(x_a, y_a) = \frac{Af_o}{2\pi f_1} \text{ RECT } \left(\frac{r_a f_o}{L_x f_1} \right) \text{ RECT } \left(\frac{y_a}{L_{r2}} \right) \quad * \tag{66}$$

The geometry of the complex amplitude incident on the apex of the cone had changed since the size of the aperture was much smaller than the cross-section of the incident illumination. Also propagation down the optical axis of the elements was the geometric projection of the preceeding apertures, since distances between elements were deep within the Fresnel diffraction region, i.e., $\lambda \ll \frac{1}{100Z}$, for plane wave illumination. Thus if the polarization of the wave is considered

$$U(x_c, y_c) = \frac{Af_o}{2\pi f_1} \text{ CIRC } \left(\frac{r_c}{L_{ra}} \right) \quad \epsilon \tag{66}$$

represented the complex amplitude and polarization of the electric vector. As the cone was illuminated, some light was reflected and some transmitted. However the base of the cone was coated with an

---

*See formula (14)

opaque film, so the transmitted light did not reach the film plane.

Resolving the complex amplitude into components perpendicular and

parallel to the plane of incidence, it can be shown that (Ref 13:219)

$$\frac{E_1''}{E_1} = - \frac{SIN\ (\phi - \phi')}{SIN\ (\phi + \phi')}$$

$$\frac{E_2''}{E_2} = \frac{TAN\ (\phi - \phi')}{TAN\ (\phi + \phi')} \tag{67}$$

Here $\frac{E_1''}{E_1}$ and $\frac{E_2''}{E_2}$, represent the perpendicular and parallel fractions

of the complex amplitudes respectively, i.e.

$$U(x_c, y_c) = \ell_1 E_1 + \ell_2 E_2$$

$$(E_1^2 + E_2^2)^{1/2} = \frac{Af_0}{2\pi f_1}\ CIRC\left(\frac{r_c}{L_{ra}}\right) \tag{68}$$

and

$$\ell = \frac{\ell_1 + \ell_2}{|\ell_1 + \ell_2|}$$

Also ϕ is the angle of incidence and ϕ' is the angle of refraction.

An inspection of Eq (67), reveals that when $\phi + \phi' = \frac{\pi}{2}$, the

parallel reflected fraction is arbitrarily small. The cone was

constructed so that the above condition was satisfied for illumina-

tion incident on the apex and along the axis of the cone. This is

Brewster's angle, which was approximately 56 degrees for the partic-

ular cone used (Ref 2:90). Consequently, there would be no intensity

83

in the film plane due to the reflected component parallel to the plane of incidence. The plane of incidence is the plane containing the normal to the reflecting surface and a vector representing the direction of propagation of the incident illumination. Thus the total intensity recorded on the film was due only to the perpendicular component of the reflected light.

Since the cone was circular in cross-section, there were an infinite number of possible incident planes. However, if the illumination was plane polarized, then the film would only record the effect of one plane of incidence, the plane of polarization. If a set of coordinate axes were imposed on the film plane such that the y-direction coincided with the plane of polarization, then the intensity in the film plane at any angle θ, from the y-axis, would be given by

$$I_1^{\prime\prime} = SIN^2 \ (\phi - \phi^\prime) [E_{1x} \ COS \ \theta + E_{1y} \ SIN \ \theta]^2 \qquad (69)$$

But since the y-axis coincides with the plane of polarization E_{1x} equals zero and

$$I_1^{\prime\prime} = SIN^2 \ (\phi - \phi^\prime) \ SIN^2 \ \theta \left[\frac{Af_o}{2\pi f_1} \ CIRC \left(\frac{r_c}{L_{ra}} \right) \right]^2 \qquad (70)$$

Thus the image on the film plane should reach a maximum at an angle of $\theta = \pm \frac{\pi}{2}$, from the plane of polarization. This implies that the null points of the image indicate the plane of polarization.

In the case of the pulsed ruby laser, the illumination was not completely plane polarized, therefore the intensity in the plane of

the film would not decrease to zero. Instead the image should exhibit two maxima (separated by π radians) and along an axis perpendicular to the axis containing the maxima, there should be two minima. Therefore the axis of minima should represent the preferred plane of polarization.

After the preferred plane of polarization had been determined, the cylinder containing the ruby crystal was rotated and subsequent images recorded until the preferred plane of polarization was aligned with the horizontal axis of the Twyman-Green interferometer for the temporal coherence experiments.

In the following photograph the maximum intensities are not equal. This was due to the misalignment of the center of the incident beam and the apex of the cone. However, it can be shown that the null points remain in the same relative position and the angle of polarization can be measured with a straight-edge with an accuracy of plus or minus two degrees (Ref 2:98).
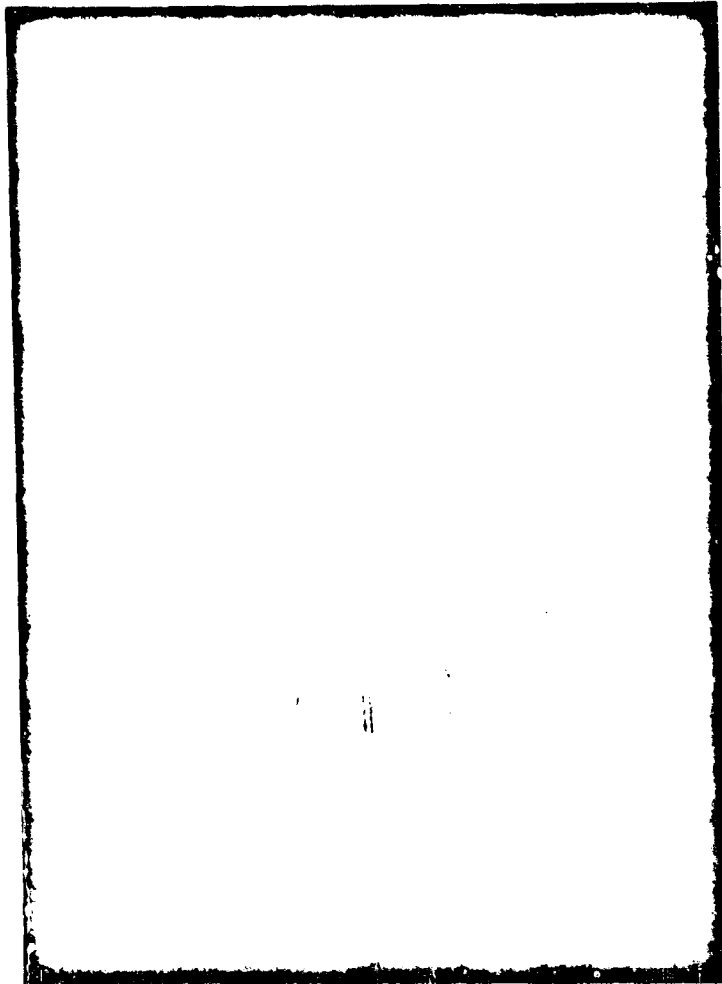
FIGURE 14

PREFERRED PLANE OF POLARIZATION

Vita

Thurston C. Holley was born on 18 November 1939 in Hawkins, Texas. He received his elementary and high school education in Houston, Texas. He attended Texas Southern University until January 1961, which was the date he entered USAF. As an airman, he completed technical training in the repair of heavy, ground, point-to-point and tropospheric scatter communications equipment while stationed at Keesler AFB, Mississippi. As a result of his selection for the Airman Education and Commissioning Program, he received a Bachelor of Science in Electrical Engineering from Colorado State University in August 1964 and was commissioned in December 1964. He then served as a radar maintenance officer in both manual AC & W and semi-automatic (SAGE) radar squadrons. Later, he served as a ground electronics inspector for the 4th Air Force (ADC) Inspector General's Staff. He was subsequently selected to attend the Air Force Institute of Technology at Wright-Patterson AFB, Ohio.

Permanent address: 4321 McKinley Street

Houston, Texas

This thesis was typed by Mrs. Jane Manemann

DOCUMENT CONTROL DATA - R & D

(Security classification of title, body of abstract and indexing annotation must be entered when the overall report is classified)

1. ORIGINATING ACTIVITY *(Corporate author)*	2a. REPORT SECURITY CLASSIFICATION
Air Force Institute of Technology (AFIT-SE) Wright-Patterson AFB, Ohio 45433	Unclassified
	2b. GROUP

3. REPORT TITLE

COHERENCE PROPERTIES OF A PULSED RUBY LASER

4. DESCRIPTIVE NOTES *(Type of report and inclusive dates)*

AFIT Thesis

5. AUTHOR(S) *(First name, middle initial, last name)*

Thurston C. Holley

Captain   USAF

6. REPORT DATE	7a. TOTAL NO. OF PAGES	7b. NO. OF REFS
June 1970	87	22

8a. CONTRACT OR GRANT NO.	9a. ORIGINATOR'S REPORT NUMBER(S)
b. PROJECT NO. N/A	GSP/PH/70-12
c.	9b. OTHER REPORT NO(S) *(Any other numbers that may be assigned this report)*
d.	

10. DISTRIBUTION STATEMENT This document is subject to special export controls and each transmittal to foreign governments or foreign nationals may be made only with prior approval of the Dean of Engineering, Air Force Institute of Technology (AFIT-SE) , Wright-Patterson AFB, Ohio 45433

11. SUPPLEMENTARY NOTES	12. SPONSORING MILITARY ACTIVITY
	Air Force Avionics Laboratory (AVTL) Wright-Patterson AFB, Ohio 45433

13. ABSTRACT

　　The coherence properties of a pulsed ruby, multi-mode laser were determined by recording the time-aver god effect of the radiation field on photographic emulsion. The recorded relative intensity distibutions were analyzed and compared with a theoretical, single mode prediction.

　　The laser beam was expanded to a one-inch diameter beam. then, with the aid of a Twyman-Green interferometer, a temporal coherence length of approximately 1.27 centimeters was observed. Also, for an aperture radius of 0.51 millimeters, in conjunction with a modified Youngs experiment, a spatial coherence length of approximately 2.2 millimeters was observed.

DD FORM 1473

14. KEY WORDS	LINK A		LINK B		LINK C	
	ROLE	WT	ROLE	WT	ROLE	WT
Pulsed ruby laser						
Coherence properties						
Multi-mode						
Photographic detection						